

# EFFICIENT REGRESSION-BASED TRAINING OF NORMALIZING FLOWS FOR BOLTZMANN GENERATORS

004  
005 **Anonymous authors**  
006 Paper under double-blind review

## ABSTRACT

009  
010 Simulation-free training frameworks have been at the forefront of the generative  
011 modelling revolution in continuous spaces, leading to large-scale diffusion and flow  
012 matching models. However, such modern generative models suffer from expensive  
013 inference, inhibiting their use in numerous scientific applications like Boltzmann  
014 Generators (BGs) for molecular conformations that require fast likelihood  
015 evaluation. In this paper, we revisit classical normalizing flows in the context of  
016 BGs that offer efficient sampling and likelihoods, but whose training via maximum  
017 likelihood is often unstable and computationally challenging. We propose REGRES-  
018 SION TRAINING OF NORMALIZING FLOWS (REGFLOW), a novel and scalable  
019 regression-based training objective that bypasses the numerical instability and  
020 computational challenge of conventional maximum likelihood training in favor of a  
021 simple  $\ell_2$ -regression objective. Specifically, REGFLOW maps prior samples under  
022 our flow to targets computed using optimal transport couplings or a pre-trained  
023 continuous normalizing flow (CNF). To enhance numerical stability, REGFLOW  
024 employs effective regularization strategies such as a new forward-backward self-  
025 consistency loss that enjoys painless implementation. Empirically, we demonstrate  
026 that REGFLOW unlocks a broader class of architectures that were previously  
027 intractable to train for BGs with maximum likelihood. We also show REGFLOW  
028 exceeds the performance, computational cost, and stability of maximum likelihood  
029 training in equilibrium sampling in Cartesian coordinates of alanine dipeptide,  
030 tripeptide, and tetrapeptide, showcasing its potential in molecular systems.

## 1 INTRODUCTION

031 The landscape of modern simulation-  
032 free generative models in continuous  
033 domains, such as diffusion mod-  
034 els and flow matching, has led to  
035 state-of-the-art generative quality  
036 across a spectrum of domains (Betker  
037 et al., 2023; Brooks et al., 2024;  
038 Huguet et al., 2024; Geffner et al.,  
039 2025). Despite the scalability of  
040 simulation-free training, generating

Table 1: Overview of various generative models and their relative trade-offs with respect to the number of inference steps, ability to provide exact likelihoods, and training objective for learning.

Method	One-step	Exact likelihood	Regression training
CNF (MLE)	✗	✓	✗
Flow Matching	✗	✓	✓
Shortcut (Frans et al., 2024)	✓	✗	✓
IMM (Zhou et al., 2025)	✓	✗	✓
NF (MLE)	✓	✓	✗
REGFLOW (ours)	✓	✓	✓

041 samples and computing model likelihoods from these model families requires computationally  
042 expensive inference—often hundreds of model calls—through the numerical simulation of the  
043 learned dynamical system. The search for efficient inference schemes has led to a new wave of  
044 approaches that seek to learn *one-step* generative models, either through distillation (Yin et al., 2024;  
045 Lu and Song, 2024; Sauer et al., 2024; Zhou et al., 2024), shortcut training (Frans et al., 2024),  
046 or Inductive Moment Matching (IMM) (Zhou et al., 2025) — methods that are able to retain the  
047 impressive sample quality of full simulation. However, many highly sensitive applications—for  
048 instance, in the natural sciences (Noé et al., 2019; Wirnsberger et al., 2020)—require more than  
049 just high-fidelity samples: they also necessitate accurate estimation of probabilistic quantities, the  
050 computation of which can be facilitated by having access to cheap and exact model likelihoods.  
051 Consequently, for one-step generative models to successfully translate to scientific applications, they  
052 must additionally provide faithful *one-step exact likelihoods* that can be used to compute scientific  
053 quantities of interest, e.g., free energy differences (Rizzi et al., 2021), using the generated samples.

Given their intrinsic capacity to compute exact likelihoods, classical normalizing flows (NF) have remained the *de facto* method for generative modelling in scientific domains (Tabak and Vanden-Eijnden,

054 2010; Tabak and Turner, 2013; Dinh et al., 2016; Rezende and Mohamed, 2015). For example, in tasks  
 055 such as equilibrium sampling of molecules, the seminal framework of Boltzmann Generators (Noé  
 056 et al., 2019) pairs a normalizing flow with an importance sampling step. Consequently, rapid and  
 057 exact likelihood evaluation is critical both for asymptotically debiasing generated samples in such  
 058 high-impact applications and for refining them via annealed importance sampling (Tan et al., 2025a;b).  
 059

060 Historically, NFs employed in conventional generative modelling domains (such as images) are trained  
 061 with the maximum likelihood estimation (MLE) objective, which has empirically lagged behind the ex-  
 062 pressiveness, scalability, and ease of training of modern continuous normalizing flows (CNFs) trained  
 063 with regression-based objectives like flow matching and stochastic interpolants (Peluchetti, 2023; Liu,  
 064 2022; Lipman et al., 2023; Albergo and Vanden-Eijnden, 2023). A key driver of the gap between classi-  
 065 cal flows and CNFs can be attributed to the MLE training objective itself, which computes the change-  
 066 of-variable formula for gradient ascent on the log-likelihood function with invertible architectures. As  
 067 a result, architectures have to balance ease of optimization with expressivity, with highly flexible archi-  
 068 tectures being highly prone to being numerically unstable (Xu and Campbell, 2023; Andrade, 2024).  
 069 For instance, in the context of Boltzmann Generators, this tension between MLE training and invertible  
 070 architectures has led to BGs that use classical flows underfitting target molecular systems in compari-  
 071 son to BGs that employ flow matching (Klein et al., 2023). However, despite the expressive power of  
 072 CNFs, inference still requires expensive numerical simulation—exact likelihood requires simulation  
 073 of the divergence, a second-order derivative. This raises the natural motivating research question:  
 074

075 **Q. Does there exist a performant training recipe for BGs with classical NFs beyond MLE?**

076 **Present work.** In this paper, we answer in the affirmative. We investigate how to train an invertible  
 077 neural network to directly match a predefined invertible function and build BGs with classical  
 078 flows. We introduce REGRESSION TRAINING OF NORMALIZING FLOWS (REGFLOW), a novel  
 079 regression-based training objective for classical normalizing flows that marks a significant departure  
 080 from the well-established MLE training objective. Our key insight is that access to coupled samples  
 081 from any invertible map is sufficient to train a generative model with a regression objective. As a  
 082 result, we can train a classical flow by learning to match in  $\ell_2$ -regression the pre-computed noise-data  
 083 pairings given by existing—both non-parametric or parametric—invertible maps. As a result, training  
 084 REGFLOW provides similar benefits to NF training as flow matching does to continuous NFs but  
 085 with the new unlocked benefit that inference provides exact likelihoods in a single step—i.e., without  
 086 numerical simulation of the probability flow ODE and thus is significantly cheaper than a CNF.  
 087

088 To train BGs using REGFLOW, we propose a variety of couplings to facilitate simple and efficient  
 089 training. We propose endpoint targets that are either: (1) outputs of a larger pretrained CNF; or (2) the  
 090 solution to a pre-computed OT map done offline as a pre-processing step. To enhance training stability  
 091 we also include a series of regularizers, and in particular, a new forward-backward self-consistency  
 092 regularizer that completely removes the need for computing the computationally-expensive Jacobian  
 093 determinant that is needed in MLE training. In each case, the designed targets are the result of  
 094 already invertible mappings, which simplifies the learning problem for NFs and enhances training  
 095 stability. Empirically, we deploy BG-based REGFLOW flows on learning equilibrium sampling  
 096 for short peptides in alanine di-, tri-, and tetrapeptide, and find even previously discarded NF for  
 097 BGs, such as affine coupling (Dinh et al., 2016) or neural spline flows (Durkan et al., 2019), can  
 098 outperform their respective MLE-trained counterpart. In particular, we demonstrate that in scientific  
 099 applications where MLE training is unsuccessful, the same BG model trained using REGFLOW  
 100 provides higher fidelity proposal samples and likelihoods. Finally, we demonstrate a completely new  
 101 method of performing Targeted Free Energy Perturbation (Wirnsberger et al., 2020) that avoids costly  
 102 energy evaluations with REGFLOW that are not possible with MLE training of normalizing flows.  
 103

## 2 BACKGROUND AND PRELIMINARIES

104 **Generative models.** A generative model can be seen as an (approximate) solution to the distribution  
 105 matching problem: given two distributions  $p_0$  and  $p_1$ , the distributional matching problem seeks to  
 106 find a push-forward map  $f_\theta : \mathbb{R}^d \rightarrow \mathbb{R}^d$  that transports the initial distribution to the desired endpoint  
 107  $p_1 = [f_\theta]_\#(p_0)$ . Without loss of generality, we set  $p_{\text{prior}} := p_0$  to be a tractable prior (typically  
 108 standard normal) and take  $p_{\text{data}} := p_1$  the data distribution, from which we have empirical samples.  
 109 We now turn our attention to solving the generative modelling problem with modelling families  
 110 that admit exact log-likelihood,  $\log p_\theta(x)$ , where  $p_\theta = [f_\theta]_\#(p_0)$ , with a particular emphasis on  
 111 normalizing flows (Tabak and Vanden-Eijnden, 2010; Tabak and Turner, 2013; Dinh et al., 2014;  
 112 2016; Rezende and Mohamed, 2015; Papamakarios et al., 2021).

108  
109

## 2.1 CONTINUOUS NORMALIZING FLOWS

110  
111  
112  
113  
114  
115  
116  
117

A CNF models the generative modelling problem as a (neural) ODE  $\frac{d}{dt}f_{t,\theta}(x) = v_{t,\theta}(f_{t,\theta}(x_t))$ . Here,  $f_\theta : [0, 1] \times \mathbb{R}^d \rightarrow \mathbb{R}^d$ ,  $(t, x_0) \mapsto x_t$  is the smooth generator and forms the solution pathway to a (neural) ordinary differential equation (ODE) with initial conditions  $f_0(x_0) = x_0$ . Furthermore,  $v_{t,\theta} : [0, 1] \times \mathbb{R}^d \rightarrow \mathbb{R}^d$  is the time-dependent velocity field associated with the (flow) map that transports particles from  $p_0$  to  $p_1$ . A CNF is an invertible map up to numerical precision, and as a result, we can compute the exact log-likelihood,  $\log p_{t,\theta}(x_t)$ , using the instantaneous change of variable formula for probability densities (Chen et al., 2018). The overall log-likelihood of a data sample,  $x_0$ , under the model can be computed as follows:

118  
119

$$\log p_{1,\theta}(x_1) = \log p_0(x_0) - \int_1^0 \nabla \cdot v_{t,\theta}(x_t) dt. \quad (1)$$

120  
121  
122  
123  
124

Maximizing the model log-likelihood in eq. (1) offers one possible method to train CNF’s but incurs costly simulation. Instead, modern scalable methods to train CNF’s employ flow matching (Lipman et al., 2023; Albergo and Vanden-Eijnden, 2023; Tong et al., 2023; Liu et al., 2023), which learns  $v_{t,\theta}$  by regressing against the (conditional) vector field associated with a designed target conditional flow everywhere in space and time, e.g., constant speed conditional vector fields.

125  
126  
127  
128  
129  
130  
131  
132  
133

**Numerical simulation.** In practice, the simulation of a CNF is conducted using a specific numerical integration scheme that can impact the likelihood estimate’s fidelity in eq. (1). For instance, an Euler integrator tends to overestimate the log-likelihood (Tan et al., 2025a), and thus it is often preferable to utilize integrators with adaptive step size, such as Dormand–Prince(4)5 (Hairer et al., 1993). In applications where estimates of the log-likelihood suffice, it is possible to employ more efficient estimators such as Hutchinson’s trace estimator to get an unbiased—yet higher variance—estimate of the divergence. Unfortunately, as we demonstrate in §3.1, such estimators are too high variance to be useful for importance sampling even in the simplest settings, and remain too computationally expensive and unreliable in larger scientific applications considered in this work.

134  
135  
136  
137  
138  
139  
140  
141  
142  
143

**One-step maps: Shortcut models.** One way to discretize an ODE is to rely on the self-consistency property of ODEs, also exploited in consistency models (Song et al., 2023), namely that jumping  $\Delta t$  in time can be constructed by following the velocity field for two half steps ( $\Delta t/2$ ). This is the core idea behind shortcut models (Frans et al., 2024) that are trained at various jumps by conditioning the vector field network on the desired step-size  $\Delta t$ . Precisely,  $f_{\text{short},t,2\Delta t}^*(x_t) = f_t^*(x_t, \Delta t)/2 + f_t^*(x'_{t+\Delta t}, \Delta t)/2$ , where  $x'_{t+\Delta t} = x_t + f_t^*(x_t, \Delta t)\Delta t$ . In their extreme, shortcut models define a one-step mapping which has been shown to generate high-quality images, but it remains an open question whether these models can reliably estimate likelihoods.

## 2.2 NORMALIZING FLOWS

144  
145  
146  
147  
148  
149  
150  
151  
152  
153  
154

The generative modelling problem can also be tackled using time-agnostic generators. One such prominent example is Normalizing Flows (NFs) (Tabak and Vanden-Eijnden, 2010; Tabak and Turner, 2013; Dinh et al., 2016; Rezende and Mohamed, 2015), which parameterize diffeomorphisms (continuously differentiable bijective functions, with a continuously differentiable inverse),  $f_\theta : \mathbb{R}^d \rightarrow \mathbb{R}^d$ . For arbitrary invertible maps  $f_\theta$ , computing the change in log probability is prohibitively expensive with cost that scales with  $O(d^3)$ . Consequently, it is popular to build  $f_\theta$  using a composition of  $M$  elementary diffeomorphisms, each with an easier to compute Jacobian determinant:  $f_\theta = f_{M-1} \circ \dots \circ f_0$  (Papamakarios et al., 2021). Through function composition, simple invertible blocks can lead to flows that are universal density approximators (Teshima et al., 2020; Ishikawa et al., 2023; Kong and Chaudhuri, 2021; Zhang et al., 2020; Bose et al., 2021), and the resulting MLE objective for training is simply:

155  
156  
157

$$\log p_\theta(x_1) = \log p_0(x_0) - \sum_{i=0}^{M-1} \log \det \left| \frac{\partial f_{i,\theta}(x_i)}{\partial x_i} \right|, \quad p_0 := \mathcal{N}(0, I). \quad (2)$$

158  
159  
160  
161

**Boltzmann Generators.** A Boltzmann Generator (BG) (Noé et al., 2019) combines a normalizing flow model,  $p_\theta$ , with an importance-sampling correction to produce i.i.d. samples from a target Boltzmann distribution  $p_{\text{target}}$ . The normalizing flow defines a tractable proposal density  $p_\theta(x)$  from which we draw  $K$  independent points  $x^{(i)} \sim p_\theta, i \in [K]$ . For each sample, we evaluate an *unnormalized* importance weight, which allow any observable  $\phi(x)$  to be consistently estimated under the target

162 measure  $p_{\text{target}}$  using self-normalized importance sampling (SNIS) (Liu, 2001; Agapiou et al., 2017):  
 163

$$\mathbb{E}_{p_{\text{target}}} [\phi(x) \bar{w}(x)] \approx \frac{\sum_{i=1}^K w(x^{(i)}) \phi(x^{(i)})}{\sum_{i=1}^K w(x^{(i)})}, \quad w(x^{(i)}) = \frac{\exp(-\mathcal{E}(x^{(i)})/k_B T)}{p_{\theta}(x^{(i)})}, \quad (3)$$

166 where  $\mathcal{E}(x)$  denotes the potential energy and  $k_B T$  are the Boltzmann constant and temperature re-  
 167 spectively. The normalized weights  $\bar{w}(x^{(i)}) = w(x^{(i)}) / \sum_j w(x^{(j)})$  can also be used to resample  
 168 the generated configurations, yielding unbiased i.i.d. draws from the desired Boltzmann distribution.  
 169

### 170 3 REGRESSION TRAINING OF NORMALIZING FLOWS

172 We seek to build one-step transport maps that both push forward samples  $x_0 \sim p_0$  to  $x_1 \sim p_1$ ,  
 173 and also permit exact likelihood evaluation. Such a condition necessitates that this learned map is  
 174 a bijective function—i.e. an invertible map—and enables us to compute the likelihood using the  
 175 change of variable formula. While using an MLE objective is always a feasible solution to learn this  
 176 map, it is often not a scalable solution for both CNFs and classical NFs. Beyond architectural choices  
 177 and differentiating through a numerical solver, learning flows using MLE is intuitively harder as  
 178 the process of learning must *simultaneously* learn the forward mapping,  $f_{\theta}$ , and the inverse mapping,  
 179  $f_{\theta}^{-1}$ , without knowledge of pairings  $(x_0, x_1) \sim \pi(x_0, x_1)$  from a coupling.

180 To appreciate this nuance, consider the set of invertible mappings  $\mathcal{I}$  and the subset of flows  $\mathcal{F} \subset \mathcal{I}$ ,  
 181 that solve the generative modelling problem. For instance, there may exist multiple ODEs (possibly  
 182 infinitely many) that push forward  $p_0$  to  $p_1$ . It is clear then that the MLE objective allows the choice  
 183 of multiple equivalent solutions  $f \in \mathcal{F}$ . However, this is precisely what complicates learning  $f_{\theta}$ ,  
 184 as *certain* solutions are harder to optimize since there is no prescribed coupling  $\pi(x_0, x_1)$  for noise  
 185  $x_0$ , and data targets  $x_1$ . That is to say, during MLE optimization of the flow  $f_{\theta}$ , the coupling  $\pi$   
 186 evolves during training as it is learned in conjunction with the flow, which can often be a significant  
 187 challenge to optimize when the pairing between noise and data is suboptimal.

188 **Regression objectives.** In order to depart from the MLE objective, we may simplify the learning  
 189 problem by first picking a solution  $f^* \in \mathcal{F}$  and fixing the coupling  $\pi^*(x_0, x_1)$  induced under  
 190 this choice, i.e.  $p_1 = [f^*]_{\#}(p_0)$ . Given privileged access to  $f^*$ , we can form a simple regression  
 191 objective that approximates this in continuous time using our choice of learnable flow:

$$\mathcal{L}(\theta) = \mathbb{E}_{t, x_0, x_1, x_t} \left[ \|f_{t, \theta}(x_t) - f_t^*(x_t)\|^2 \right], \quad (4)$$

193 where  $(x_0, x_1) \sim \pi^*(x_0, x_1)$  and  $x_t \sim p_t(\cdot | x_0, x_1)$  is drawn from a known conditional noising  
 194 kernel such as a Gaussian distribution. We note that the regression objective in eq. (4) is more general  
 195 than just flows in  $\mathcal{I}$ , and, at optimality, the learned function behaves like  $f_t^*$  on the support of  $p_0$ ,  
 196 under mild regularity conditions. We formalize this intuition more precisely in the next proposition.  
 197

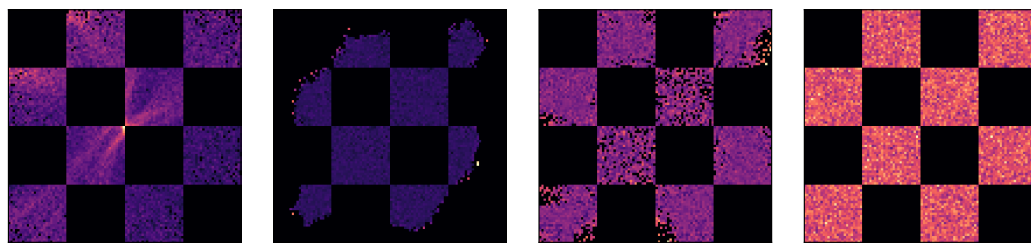
198 **Proposition 1.** Suppose that  $f_t^*$  is invertible for all  $t$ , that  $(f_t^*)^{-1}$  is continuous for all  $t$ . Then,  
 199 as  $\mathcal{L}(\theta) \rightarrow 0$ , it holds that  $((f_t^*)^{-1} \circ f_{t, \theta})(x) \rightarrow x$  for almost all (with respect to  $p_0$ )  $x$ .

200 The proof for proposition 1 can be found in §A, and illuminates that solving the original generative  
 201 modelling problem via MLE can be re-cast as a *matching* problem to a known invertible function  
 202  $f^*$ . Indeed, many existing generative models already fit into this general regression objective based  
 203 on the choice of  $f^*$ , such as conditional flow matching (CFM) (Tong et al., 2023), rectified flow (Liu  
 204 et al., 2023), and (perfect) shortcut models (Frans et al., 2024). This proposition also shows why  
 205 these models work as generative models: they converge in probability to the prespecified map.

#### 206 3.1 WARMUP: ONE-STEP GENERATIVE MODELS WITHOUT LIKELIHOOD

208 As there exist powerful one-step generative models in image applications, it is tempting to consider  
 209 whether they can be used for BG applications requiring likelihoods. As a warmup, we investigate the  
 210 use of current state-of-the-art one-step generative models in shortcut models (Frans et al., 2024) and In-  
 211 ductive Moment Matching (IMM) (Zhou et al., 2024) through a simple experiment (see §B for details).

212 **Synthetic experiments.** We instantiate both model classes on a simple generative modelling problem,  
 213 where the data is a checkerboard density. In fig. 1, we plot the results and observe, that non-invertible  
 214 shortcuts and IMM models are imperfect at learning the target and are unable to be corrected to  
 215  $p_{\text{synth}}$  after resampling. However, when IMM is used to train an NF (Durkan et al., 2019), we see  
 samples that almost perfectly match  $p_{\text{synth}}$ —but such an approach is not scalable (§B.2).



(a) Non-invertible shortcut. (b) Non-invertible IMM. (c) IMM with an NF. (d) Ground truth.

Figure 1: Evaluation of IMM and shortcut models with exact likelihood on the synthetic checkerboard experiment. Depictions are provided of the 2D histograms after self-normalizing importance sampling is used.

This puts spotlight on a counter-intuitive question given proposition 1: *Why do shortcut models have incorrect likelihoods?* While proposition 1 implies pointwise convergence of  $f_\theta$  to  $f^*$ , this does not imply convergence or regularity of the gradients of  $f_\theta$ , and thus shortcut models can still achieve high quality generations without the need to provide faithful likelihoods.

**Insufficiency of uniform convergence.** One-step maps are trained to converge pointwise to  $f_\theta \rightarrow f^*$  on a sub-domain  $D \subseteq \mathbb{R}^d$ . However, this does not imply pointwise convergence of gradients  $\nabla f_\theta \rightarrow \nabla f^*$ . For instance, consider the following toy example:  $f_m(x) = \frac{1}{m} \sin(mx) + x$  and  $f^*(x) = x$ . As  $m \rightarrow \infty$ ,  $f_m$  converges uniformly to  $f^*$ ; however, the gradient  $\nabla f_m(x) = \cos(mx)$  does not converge. Importantly, this means that while  $f_\theta$  would produce increasingly accurate generations, its likelihoods derived through eq. (2) may not converge to those of the base model.

### 3.2 TRAINING NORMALIZING FLOWS USING REGRESSION

We now outline our REGFLOW framework to train a one-step map for a classical NF. To remedy the issue found in shortcut models and IMM in section 3.1, we judiciously choose  $f_\theta$  to be an already exactly invertible mapping—i.e., a classical NF. Since NFs are one-step maps by construction, eq. (4) is instantiated using a simple regression objective follows:

$$\mathcal{L}(\theta) = \mathbb{E}_{x_0, x_1} \left[ \|f_{1, \theta}(x_0) - f_1^*(x_0)\|^2 \right] + \lambda_r \mathcal{R} = \mathbb{E}_{x_0, x_1} \left[ \|\hat{x}_1 - x_1\|^2 \right] + \lambda_r \mathcal{R}, \quad (5)$$

where  $\mathcal{R}$  is a regularization strategy and  $\lambda_r \in \mathbb{R}^+$  is the strength of regularization. Explicit in eq. (5) is the need to procure *one-step* targets  $x_1 = f_1^*(x_0)$  from a known invertible mapping  $f_1^*$ . We outline the choice of such functions in §3.3. We also highlight that the one-step targets in eq. (5) differ from the typical flow matching objective where the continuous targets  $f_{t, \text{cfm}}^* = \frac{\partial}{\partial t} p_t(x_t | x_0, x_1)$  (see §A.3 for a discussion). Consequently, for NFs that are universal density approximators (Teshima et al., 2020; Kong and Chaudhuri, 2021; Zhang et al., 2020), the learning problem includes a feasible solution.

**Training recipe.** We provide the full training pseudocode in algorithm 1. In practice, we find that  $f^*$  is often ill-conditioned, with the target distribution often centered around some lower-dimensional subspace of  $\mathbb{R}^d$  similar to prior work (Zhai et al., 2024). This may cause  $f_\theta$  to become numerically ill-conditioned. To combat this, we use three tricks to maintain numerical stability. Specifically, we regularize the loss function, add small amounts of Gaussian noise to the target distribution similar to Hui et al. (2025); Zhai et al. (2024), and, finally, add weight decay to our optimizer.

**Speedup from uni-directional flow training and inference.** For some flow types these are roughly equivalent (RealNVP or Jet) in computation time. However, for some flows such as autoregressive flows (e.g. NSF), the network  $f(x)$  is substantially faster to evaluate than its inverse  $f^{-1}(x)$ . In standard maximum likelihood training of normalizing flows, the model is trained with passes from data to noise. This is then reversed during generation with passes from noise to data. In REGFLOW, inference and training can be done from noise to data. This means substantially faster inference can be achieved by training autoregressive flows where the fast direction is oriented from noise to data.

**Regularization Strategies.** In principle, classical normalizing flows can be trained using a standalone regression objective that directly maps latents to data. In practice, we observe that regression training alone can impact numerical invertibility—a similar phenomenon to that observed in MLE-trained normalizing flows (Xu and Campbell, 2023; Andrade, 2024). This adversely impacts re-weighted samples as the NF becomes increasingly numerically unstable. To remedy this, we introduce two regularization strategies, one using the log-determinant of the Jacobian (see eq. 6), while the other

270 does not, resembling a cycle-consistency loss using forward-backward regularization (see eq. 7):  
 271

$$\mathcal{L}_{\text{log-det}} = \|f_\theta(x_0) - x_1\|_2^2 + \lambda_r (\log |\det(J_\theta(x))|)^2 \quad (6)$$

$$\mathcal{L}_{\text{fwd-bwd}} \triangleq \|f_\theta(x_0) - x_1\|_2^2 + \lambda_r \|f_\theta^{-1}(f_\theta(x_0)) - x_0\|_2^2. \quad (7)$$

272 The first regularization strategy uses the same log determinant that is needed in the change of variable  
 273 formula, which comes at no additional computational cost for the architectures we experiment with.  
 274 Intuitively, this penalizes the flow map from collapsing to a point as it regularizes against sharp mass  
 275 placements, which is what a determinant geometrically computes. The second regularizer is a new  
 276 forward-backward self-consistency regularizer that ensures invertibility at the output level, but at  
 277 double the computational cost. However, interestingly, since it does not require the Jacobian, it opens  
 278 up potential directions for less constrained architectures. For our purposes, we find both of these  
 279 regularizers accomplish our aim of avoiding collapse and maintaining invertibility.  
 280

---

**Algorithm 1** REGRESSION TRAINING OF NORMALIZING FLOWS
 

---

281 **Input:** Prior  $p_0$ , empirical samples from  $p_1$ , regularization weight  $\lambda_r$ , noise scale  $\lambda_n$ , network  $f_\theta$   
 282  
 1: **while** training **do**  
 2:    $(x_0, x_1) \sim \pi(x_0, x_1)$   $\triangleright$  Sample batches of size  $b$  i.i.d. from the dataset  
 3:    $x_1 \leftarrow x_1 + \lambda_n \cdot \varepsilon$ , with  $\varepsilon \sim \mathcal{N}(0, I)$   $\triangleright$  Add scaled noise to targets  
 4:    $\mathcal{L}(\theta) \leftarrow \|f_\theta(x_0) - x_1\|_2^2 + \lambda_r \mathcal{R}$   $\triangleright$  Loss with regularization  
 5:    $\theta \leftarrow \text{Update}(\theta, \nabla_\theta \mathcal{L}(\theta))$   
 6: **return**  $f_\theta$

---

291  
 292   3.3 REGFLOW TARGETS  
 293

294 To construct useful one-step targets in REGFLOW, we must find a discretization of an invertible  
 295 function—e.g., an ODE solution—at longer time horizons. More precisely, we seek a discretization  
 296 of an ODE such that each time point  $t + \Delta t$  where the regression objective evaluated corresponds  
 297 to a true invertible function  $f_{t+\Delta t}^*$ . Consequently, if we have access to an invertible map such that  
 298  $t + \Delta t = 1$ , we can directly regress our parametrized function as a one-step map,  $f_{0,\theta}(x_0) = \hat{x}_1$ .  
 299 This motivates the search and design of other invertible mappings that give us invertibility at longer  
 300 time horizons, for which we give two examples next.

301 **Optimal transport targets.** Optimal transport in continuous space between two distributions  
 302 defines a continuous and invertible transformation expressible as the gradient of some convex  
 303 function (Villani, 2021; Peyré and Cuturi, 2019). This allows us to consider the invertible OT plan:

$$f_{\text{ot}}^* = \arg \min_T \int T(x) c(x, T(x)) dp_0(x) \text{ s.t. } T_{\#}(p_0) = p_1, \quad (8)$$

304 where  $c : \mathbb{R}^d \times \mathbb{R}^d \rightarrow \mathbb{R}$  is the OT cost and  $T : \mathbb{R}^d \rightarrow \mathbb{R}^d$  is a transport map. We note that this  
 305 map is interesting as it requires no training; however, exact OT runs in  $\tilde{O}(n^3)$  time and  $O(n^2)$  space,  
 306 which makes it challenging to scale to large datasets. Furthermore, we highlight that this differs from  
 307 OT-CFM (Tong et al., 2023), which uses mini-batches to approximate the OT-plan. Nevertheless,  
 308 in applicable settings, full batch OT acts as a one-time offline pre-processing step for training  $f_\theta$ .

309 **Reflow targets.** Another strategy to obtain samples from an invertible map is to use a pretrained  
 310 CNF, also known as *reflow* (Liu, 2022). Specifically, we have that:

$$f_{\text{reflow}}^*(x_0) = x_0 + \int_0^1 v_t^*(x_t) dt = x_1. \quad (9)$$

311 In other words, the one-step invertible map is obtained from a pre-trained CNF  $v_t^*$ , from which we  
 312 collect a dataset of noise-target pairs, effectively forming  $\pi^*(x_0, x_1)$ . We now prove that training  
 313 on reflow targets with REGFLOW reduces the Wasserstein distance to the  $p_1$ .

314 **Proposition 2.** Let  $p_{\text{reflow}}$  be a pretrained CNF generated by the vector field  $v_t^*$ , real numbers  
 315  $(L_t)_{t \in [0,1]}$  such that  $v_t^*$  is  $L_t$ -Lipschitz for all  $t \in [0, 1]$ , and a NF  $f_\theta^{\text{ref}}$  trained using Eq. 5 by

324 regressing against  $f_{\text{reflow}}^*(x_0)$ , where  $x_0 \sim \mathcal{N}(0, I)$ . Then, writing  $p_\theta^{\text{ref}} := \text{Law}(f_\theta^{\text{ref}}(x_0))$ , we have:

325

$$326 \quad \mathcal{W}_2(p_1, p_\theta) \leq K \exp \left( \int_0^1 L_t dt \right) + \epsilon, \quad K \geq \int_0^1 \mathbb{E} \left( [\|v_t^*(x_t) - v_{t,\text{true}}(x_t)\|_2^2] \right)^{\frac{1}{2}} dt, \quad (10)$$

327

328 where  $K$  is the  $\ell_2$  approximation error between the velocity field of the CNF and the ground  
329 truth generating field  $v_t^*$ ,  $\epsilon^2 = \mathbb{E}_{x_0, x_1} \left[ \|f_{\text{reflow}}^*(x_0) - f_\theta^{\text{ref}}(x_0)\|_2^2 \right]$ .  
330

331 The proof for proposition 2 is provided in §A. Intuitively, the first term captures the approximation  
332 error of the pretrained CNF to the actual data distribution  $p_1$ , and the second term captures the  
333 approximation gap between the flow trained using REGFLOW to the reflow targets obtained via  $p_{\text{reflow}}$ .

334 While these two cases represent interesting instantiations of  $f^*$ , there exist many other possible  
335 procedures for obtaining  $f^*$ . We investigate the theoretical properties for  $f^*$  in appendix A.4 to  
336 provide guidance for those who wish to investigate other targets.

337  
338 Table 2: Quantitative results on alanine dipeptide (ALDP), tripeptide (AL3), and tetrapeptide (AL4) reported as  
339 mean  $\pm$  standard deviation over three seeds.

340

Datasets $\rightarrow$	Dipeptide (ALDP)			Tripeptide (AL3)			Tetrapeptide (AL4)		
	ESS $\uparrow$	$\mathcal{E}\text{-}\mathcal{W}_1 \downarrow$	$\mathbb{T}\text{-}\mathcal{W}_2 \downarrow$	ESS $\uparrow$	$\mathcal{E}\text{-}\mathcal{W}_1 \downarrow$	$\mathbb{T}\text{-}\mathcal{W}_2 \downarrow$	ESS $\uparrow$	$\mathcal{E}\text{-}\mathcal{W}_1 \downarrow$	$\mathbb{T}\text{-}\mathcal{W}_2 \downarrow$
Algorithm $\downarrow$									
NSF (MLE)	<b>0.055 <math>\pm</math> 0.012</b>	13.797 $\pm$ 2.713	1.243 $\pm$ 0.103	0.024 $\pm$ 0.004	17.596 $\pm$ 1.21	1.665 $\pm$ 0.180	<b>0.016 <math>\pm</math> 0.003</b>	20.886 $\pm$ 1.930	3.885 $\pm$ 0.410
NSF (REGFLOW)	0.035 $\pm$ 0.004	<b>0.501 <math>\pm</math> 0.011</b>	<b>0.951 <math>\pm</math> 0.054</b>	0.031 $\pm$ 0.018	<b>0.853 <math>\pm</math> 0.105</b>	1.577 $\pm$ 0.140	0.011 $\pm$ 0.003	<b>3.277 <math>\pm</math> 0.546</b>	<b>2.342 <math>\pm</math> 0.102</b>
Res-NVP (MLE)	<1e-4	>1e3	>30	<1e-4	>1e3	>30	<1e-4	>1e3	>30
Res-NVP (REGFLOW)	<b>0.035 <math>\pm</math> 0.008</b>	<b>2.104 <math>\pm</math> 0.586</b>	<b>0.812 <math>\pm</math> 0.121</b>	<b>0.025 <math>\pm</math> 0.006</b>	<b>3.241 <math>\pm</math> 0.301</b>	<b>1.881 <math>\pm</math> 0.205</b>	<b>0.013 <math>\pm</math> 0.004</b>	<b>2.705 <math>\pm</math> 0.306</b>	<b>2.117 <math>\pm</math> 0.331</b>
Jet (MLE)	<1e-4	>1e3	>30	<1e-4	>1e3	>30	<1e-4	>1e3	>30
Jet (REGFLOW)	<b>0.055 <math>\pm</math> 0.006</b>	<b>4.193 <math>\pm</math> 1.016</b>	<b>0.801 <math>\pm</math> 0.076</b>	<1e-4	>1e3	<b>3.644 <math>\pm</math> 0.358</b>	<1e-4	>1e3	>30

## 346 4 EXPERIMENTS

347 We evaluate NFs trained with REGFLOW on three molecular systems: alanine dipeptide (ALDP),  
348 alanine tripeptide (AL3), and alanine tetrapeptide (AL4). These peptides are a standard benchmark  
349 for testing generative models in computational chemistry. We assess the models on two key tasks:  
350 equilibrium conformation sampling and targeted free energy prediction (TFEP) (Wirnsberger et al.,  
351 2020). Through these experiments, we show that REGFLOW outperforms the conventional maximum  
352 likelihood estimation (MLE) training for NFs in these scientific applications.

353 **Setup.** We test three different architectures: RealNVP with a residual network parametrization (Dinh  
354 et al., 2016), neural spline flows (NSF) (Durkan et al., 2019), and Jet (Kolesnikov et al., 2024),  
355 across three different molecular systems (ALDP, AL3, and AL4) of increasing size and compare  
356 the performance of the same invertible architecture trained using MLE, and using REGFLOW. We  
357 report: Effective Sample Size (ESS); the 1-Wasserstein distance on the energy distribution; and the  
358 2-Wasserstein distance on the main dihedral angles as described in §C with additional results in §D.

359 **Main results.** We report our main quantitative results in table 2 and observe that REGFLOW with  
360 reflow targets consistently outperforms MLE training of NFs across all architectures on both  $\mathcal{E}\text{-}\mathcal{W}_1$   
361 and  $\mathbb{T}\text{-}\mathcal{W}_2$  metrics, and slightly underperforms MLE training on ESS. However, this can be justified  
362 by the mode collapse that happens in MLE training as illustrated in the Ramachandran plots for  
363 alanine dipeptide fig. 2, which artificially increases ESS. Examining the energy histogram plots  
364 in fig. 2 we observe that NFs trained using REGFLOW more closely match the true energy distribution.  
365 We also illustrate these improvements across metrics when using OT targets over reflow, as shown  
366 Appendix fig. 9. Our results clearly demonstrate that REGFLOW is often a compelling alternative to  
367 MLE training in BGs for all analyzed NF architectures, and allows training of architectures that were  
368 previously untrainable with MLE training.

369 **REGFLOW leads to faster training and inference.** We  
370 note that NFs trained with REGFLOW are substantially  
371 faster at computing likelihoods compared to their MLE-  
372 trained counterparts, except for cases where the NF has  
373 an analytical inverse (Res-NVP, Jet) due to the reversal  
374 of the flow. For autoregressive flows like NSF, where  
375 the reverse pass is far slower to compute than the for-  
376 ward pass, we observe the maximum benefit: REGFLOW  
377 enables nearly a 34 $\times$  speedup in inference compared to the equivalent MLE-trained NF, as seen in  
378 Tab. 3. We also compare performance relative to continuous normalizing flows (CNFs), which require

379  
380 Table 3: Inference efficiency comparisons.  
381 Time to compute likelihoods for 200k samples.

Models $\rightarrow$	Dipeptide (ALDP)			
	MLE	REGFLOW	CFM	Speed Up
NSF	277.00	8.18	N/A	33.8 $\times$
Res-NVP	3.64	3.51	N/A	1.03 $\times$
Jet	67.63	60.43	N/A	1.11 $\times$
CNF DiT	N/A	N/A	26969.80	N/A

378  
379  
380  
381  
382  
383

Table 4: Training time comparison between MLE and REGFLOW for alanine dipeptide.

Metric $\downarrow$	MLE		REGFLOW	
	OT	CNF		
$\mathcal{E}\mathcal{W}_1 = 7.090$	10h10	6h54	7h23	
$\mathbb{T}\mathcal{W}_2 = 1.368$	12h17	7h32	7h56	

384  
385  
386  
387  
388  
389  
390  
391  
392  
393  
394

Table 5: ALDP with various regularization strategies.

Models $\rightarrow$	Dipeptide (ALDP)		
	Algorithm $\downarrow$	ESS $\uparrow$	$\mathcal{E}\mathcal{W}_1 \downarrow$
NSF (MLE)	<b>0.055 <math>\pm</math> 0.012</b>	13.797 $\pm$ 2.713	1.243 $\pm$ 0.103
NSF (REGFLOW w/o reg)	0.032 $\pm$ 0.008	0.604 $\pm$ 0.045	1.083 $\pm$ 0.109
NSF (REGFLOW w/ logdets)	0.036 $\pm$ 0.007	0.519 $\pm$ 0.021	0.958 $\pm$ 0.074
NSF (REGFLOW w/ fwd-bwd)	0.035 $\pm$ 0.004	<b>0.501 <math>\pm</math> 0.011</b>	<b>0.951 <math>\pm</math> 0.054</b>
Res-NVP (MLE)	$< 10^{-4}$	$> 10^3$	$> 30$
Res-NVP (REGFLOW w/o reg)	0.033 $\pm$ 0.010	2.948 $\pm$ 0.457	1.179 $\pm$ 0.218
Res-NVP (REGFLOW w/ logdets)	0.032 $\pm$ 0.008	2.310 $\pm$ 0.411	<b>0.796 <math>\pm</math> 0.109</b>
Res-NVP (REGFLOW w/ fwd-bwd)	<b>0.035 <math>\pm</math> 0.008</b>	<b>2.104 <math>\pm</math> 0.586</b>	0.812 $\pm$ 0.121
Jet (MLE)	$< 10^{-4}$	$> 10^3$	$> 30$
Jet (REGFLOW w/o reg)	0.053 $\pm$ 0.007	9.707 $\pm$ 1.843	1.224 $\pm$ 0.181
Jet (REGFLOW w/ logdets)	0.051 $\pm$ 0.004	6.349 $\pm$ 1.412	0.872 $\pm$ 0.065
Jet (REGFLOW w/ fwd-bwd)	<b>0.055 <math>\pm</math> 0.006</b>	<b>4.193 <math>\pm</math> 1.016</b>	<b>0.801 <math>\pm</math> 0.076</b>

integrating the divergence of the vector field—this makes likelihood evaluation extremely expensive compared to discrete NFs. We observe that CNF inference with likelihoods is approximately  $450\times$  more expensive than our slowest NF (Jet) and  $7700\times$  more expensive than our fastest NF (Res-NVP).

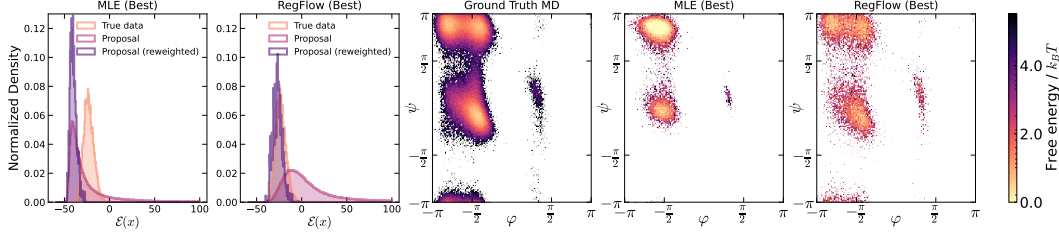


Figure 2: Energy distributions and **resampled** Ramachandran plots for alanine dipeptide. **(left to right):** Energy distribution of most best MLE-trained NF; energy distribution of best REGFLOW; ground truth MD data torsion angle distribution; best MLE-trained model Ramachandran plot; best REGFLOW Ramachandran plot.

Next, we contrast the training times between MLE and REGFLOW, accounting for: (1) CNF training or OT map pre-computation; (2) sample generation from the CNF; and (3) REGFLOW training until its performance exceeds MLE. Across all settings, REGFLOW consistently outperforms MLE. Specifically, we observe that achieving superior performance on  $\mathcal{E}\mathcal{W}_1$  requires  $\sim 27\%$  less time with REGFLOW, while on  $\mathbb{T}\mathcal{W}_2$ , the speedup is closer to  $\sim 35\%$ . We also compare the training times between MLE and REGFLOW across all peptide systems. In fig. 3, we illustrate how the energy varies during training using REGFLOW; the dotted lines symbolize the best energy using the MLE-trained NSF on the validation set. Here, we see that the crossover between REGFLOW and MLE occurs after  $\sim 1h20$ ,  $\sim 1h20$ , and  $\sim 2h40$ , for REGFLOW to outperform MLE on the dipeptide, tripeptide, and tetrapeptide, respectively. Conversely, MLE training took  $\sim 10h10$ ,  $\sim 11h20$ , and  $\sim 11h40$  using the dipeptide, tripeptide, and tetrapeptide, respectively. These studies further validate the potential for REGFLOW to serve as an efficient and effective alternative to MLE.

**Alternative regularization strategies.** We investigate the impact of different regularization strategies to prevent numerical collapse for REGFLOW in table 5. We consider no regularization (w/o reg), regularization of the magnitude of the log determinant of the Jacobian (w/ logdets), and a direct invertibility penalization (forward-backward). For our usecase, the Jacobian comes at no extra cost and is therefore the most efficient. The forward-backward regularizer enforces cycle consistency by performing a forward pass of the NF, followed by a reverse pass on the same generated samples, and computing the  $\ell_2$  distance between the reconstructed priors. This

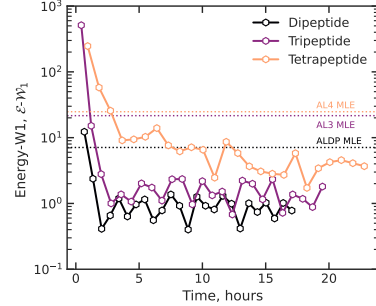


Figure 3: **Training time required for REGFLOW to outperform the most performant MLE model (NSF).**

is at least twice as expensive as the logdet regularization for our use case, however it does perform quite well, and interestingly opens up the possibility for more flexible architectures. All regularizations outperform MLE, and the logdet regularization offers the best tradeoff between performance and speed for our usecase, so we use that regularization for the remainder of our experiments.

**Ablations.** In table 6, we report REGFLOW using OT targets and various amounts of generated reflow targets—a unique advantage of using reflow as the invertible map. As observed, each target choice improves over MLE, outside of ESS for NSF. Importantly, we find that using more samples in reflow consistently improves performance metrics for all architectures. In fig. 4, we show how performance increases with the number reflow samples and we ablate the impact of regularization. We find performance improvements with increasing regularization, up to around  $10^{-6} \leq \lambda_r \leq 10^{-5}$ . Regularizing beyond this is sufficient to ensure empirical invertibility based on validation loss of  $\mathcal{L}_{fwd-bck} < 10^{-4}$ , but hampers generation performance.

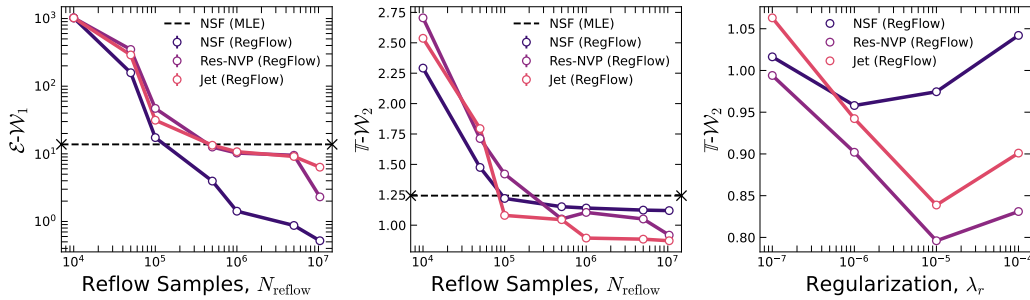


Figure 4: **Left and center:** Ablations demonstrating performance improvements with an increasing number of reflow samples. **Right:** Increasing regularization improves  $\mathbb{T}\mathcal{W}_2$  up to a certain point, beyond which numerical invertibility is guaranteed but the regression objective, and subsequently, sample quality, is adversely impacted.

**Targeted Free Energy Perturbation.** Accurate calculations of the free energy difference between two metastable states of a physical system is both ubiquitous and of profound importance in the natural sciences. One approach to tackling this problem is Free Energy Perturbation (FEP) which exploits Zwanzig’s identity:  $\mathbb{E}_A [e^{-\beta \Delta U}] = e^{-\beta \Delta F}$ , where  $\Delta F = F_B - F_A$  is the Helmholtz free energy difference between two metastable states  $A$  and  $B$  (Zwanzig, 1954). Targeted Free Energy Perturbation (TFEP) improves over FEP by using NFs to learn an invertible map using MLE to increase the distributional overlap between states  $A$  and  $B$  (Wirnsberger et al., 2020; Moqvist et al., 2025); however, this can be challenging for several reasons. NFs are difficult to learn, especially when the energy function is expensive to compute, or the states occupy small areas.

We propose a new TFEP method that does not require energy function evaluations during training. By using REGFLOW, we can train the NF solely based on samples from states  $A$  and  $B$ . This enables TFEP, where energy evaluations may be costly—a new possibility that is distinct from NFs trained using MLE. To demonstrate this application of REGFLOW, we train an NF solely from samples from two modes of ALDP (see fig. 5) and use OT targets which avoid any energy function evaluation. We include a reference using the DiT CNF—trained to map between meta-stable states—which also

Table 6: Ablations on target types and amount of reflow targets on ALDP.

Datasets →	Dipeptide (ALDP)		
	Algorithm ↓	ESS ↑	$\mathcal{E}\mathcal{W}_1 \downarrow$
NSF (MLE)	<b>0.055</b>	13.80	1.243
NSF (REGFLOW @ 100k CNF)	0.016	17.39	1.232
NSF (REGFLOW @ 10.4M CNF)	0.035	<b>0.501</b>	<b>0.951</b>
NSF (REGFLOW @ OT)	0.003	0.604	2.019
Res-NVP (MLE)	< $10^{-4}$	$> 10^3$	> 30
Res-NVP (REGFLOW @ 100k CNF)	0.009	46.93	1.155
Res-NVP (REGFLOW @ 10.4M CNF)	<b>0.035</b>	2.104	<b>0.812</b>
Res-NVP (REGFLOW @ OT)	0.006	<b>0.699</b>	1.969
Jet (MLE)	< $10^{-4}$	$> 10^3$	> 30
Jet (REGFLOW @ 100k CNF)	0.017	31.42	1.081
Jet (REGFLOW @ 10.4M CNF)	<b>0.051</b>	4.193	<b>0.801</b>
Jet (REGFLOW @ OT)	0.003	<b>2.534</b>	1.913

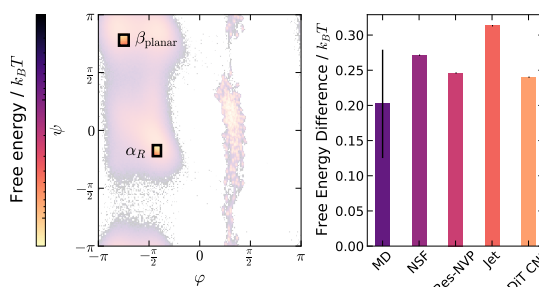


Figure 5: **Left:** The  $\beta_{\text{planar}}$  and  $\alpha_R$  conformation states; **Right:** REGFLOW’s ability to learn free energy differences.

486 achieves similar predictions, albeit taking nearly three orders of magnitude longer to compute. We  
 487 find we can achieve high-quality free energy estimation in comparison to ground truth Molecular  
 488 Dynamics (MD) using only samples during training, as illustrated in fig. 5. We believe this is a  
 489 promising direction for future applications of free energy prediction.

## 491 5 RELATED WORK

492 **Exact likelihood generative models.** NFs are generative models with invertible architectures  
 493 (Rezende and Mohamed, 2015; Dinh et al., 2016) that produce *exact* likelihoods for any given  
 494 points. Common models include RealNVP (Dinh et al., 2016), neural spline flows (Durkan et al.,  
 495 2019), and Glow (Kingma and Dhariwal, 2018). Jet (Kolesnikov et al., 2024) and TarFlow (Zhai  
 496 et al., 2024) are examples of transformer-based normalizing flows. Aside from Jet and Tarflow, NFs  
 497 have generally underperformed compared to diffusion models and flow matching methods (Ho et al.,  
 498 2020; Lipman et al., 2023; Albergo et al., 2023; Liu, 2022), partly due to the high computational  
 499 cost of evaluating the log-determinants of Jacobians at each training step.

500 **Few-step generative models.** To avoid costly inference, few-step generative models were introduced  
 501 as methods to accelerate the simulation of diffusion and CNFs. Common examples include DDIM  
 502 (Song et al., 2022) and consistency models (Song et al., 2023), which introduced a new training  
 503 procedure that ensured the model’s endpoint prediction remained consistent. Recently, flow  
 504 maps (Boffi et al., 2024; 2025; Song and Dhariwal, 2023; Lu and Song, 2024; Geng et al., 2024;  
 505 2025; Sabour et al., 2025) have improved upon this paradigm. Other lines of work proposed related  
 506 but different training objectives, generalizing consistency training (Frans et al., 2024; Zhou et al.,  
 507 2025; Kim et al., 2024; Heek et al., 2024). Beyond diffusion and FM, residual networks (He et al.,  
 508 2015) are a class of neural networks that are invertible if the Lipschitz constant of  $f_\theta$  is at most  
 509 one (Behrmann et al., 2019). The log-determinant of the Jacobian is then approximated by truncating  
 510 a series of traces (Behrmann et al., 2019)—an approximation improved in Chen et al. (2020).

## 511 6 CONCLUSION

512 In this work, we present REGFLOW, a method for generating high-quality samples alongside exact  
 513 likelihoods in a single step. Using a base coupling between the dataset samples and the prior, provided  
 514 by either pre-computed optimal transport or a base CNF, we can train a classical NF using a simple  
 515 regression objective that avoids computing Jacobians at training time, as opposed to typical MLE  
 516 training. In theory and practice, we have shown that the learned model produces faithful samples,  
 517 the likelihoods of which empirically allow us to produce state-of-the-art results on several molecular  
 518 datasets, using importance-sampling resampling. Limitations include the quality of the proposal  
 519 samples, which substantially improve on MLE-trained NFs, but are not on par with state-of-the-art  
 520 CNFs or variants thereof. Moreover, while producing accurate and high-quality likelihoods, they do  
 521 not, in theory, match those of the base coupling, which can be a desirable property.

522  
 523  
 524  
 525  
 526  
 527  
 528  
 529  
 530  
 531  
 532  
 533  
 534  
 535  
 536  
 537  
 538  
 539

540   **ETHICS STATEMENT**  
541542   This paper is primarily methodological, presenting theoretical developments without direct exper-  
543   imental implementation or associated ethical considerations; however, we advise due caution for  
544   future beneficiaries of our work in their potentially sensitive application domains.545   **REPRODUCIBILITY STATEMENT**  
546547   We have made numerous efforts to ensure the reproducibility of our work. The main paper provides  
548   detailed descriptions of the proposed methods and evaluation protocols. Additionally, in our Ap-  
549   pendix, we include extensive details on data normalization, the MD datasets used for training, model  
550   architectures and sizes, training configurations, and our choice of regularization hyperparameters.  
551   Further, all assumptions and methodological choices are explicitly documented, and we plan to  
552   publicly release all the developed code upon acceptance.553  
554  
555  
556  
557  
558  
559  
560  
561  
562  
563  
564  
565  
566  
567  
568  
569  
570  
571  
572  
573  
574  
575  
576  
577  
578  
579  
580  
581  
582  
583  
584  
585  
586  
587  
588  
589  
590  
591  
592  
593

594 REFERENCES  
595

596 S. Agapiou, O. Papaspiliopoulos, D. Sanz-Alonso, and A. M. Stuart. Importance sampling: Intrinsic  
597 dimension and computational cost. *Statistical Science*, pages 405–431, 2017.

598 M. S. Albergo and E. Vanden-Eijnden. Building normalizing flows with stochastic interpolants.  
599 *International Conference on Learning Representations (ICLR)*, 2023.

600 M. S. Albergo, N. M. Boffi, and E. Vanden-Eijnden. Stochastic interpolants: A unifying framework  
601 for flows and diffusions. *arXiv preprint 2303.08797*, 2023.

602 D. Andrade. Stable training of normalizing flows for high-dimensional variational inference. *arXiv  
603 preprint arXiv:2402.16408*, 2024.

604 J. Behrmann, W. Grathwohl, R. T. Q. Chen, D. Duvenaud, and J.-H. Jacobsen. Invertible residual  
605 networks, 2019. URL <https://arxiv.org/abs/1811.00995>.

606 J. Benton, G. Deligiannidis, and A. Doucet. Error bounds for flow matching methods. *arXiv preprint  
607 arXiv:2305.16860*, 2023.

608 J. Betker, G. Goh, L. Jing, T. Brooks, J. Wang, L. Li, L. Ouyang, J. Zhuang, J. Lee, Y. Guo,  
609 et al. Improving image generation with better captions. *Computer Science*. <https://cdn.openai.com/papers/dall-e-3.pdf>, 2(3):8, 2023.

610 N. M. Boffi, M. S. Albergo, and E. Vanden-Eijnden. Flow map matching. *arXiv preprint  
611 arXiv:2406.07507*, 2, 2024.

612 N. M. Boffi, M. S. Albergo, and E. Vanden-Eijnden. How to build a consistency model: Learning  
613 flow maps via self-distillation, 2025. URL <https://arxiv.org/abs/2505.18825>.

614 A. J. Bose, M. Brubaker, and I. Kobyzev. Equivariant finite normalizing flows. *arXiv preprint  
615 arXiv:2110.08649*, 2021.

616 T. Brooks, B. Peebles, C. Holmes, W. DePue, Y. Guo, L. Jing, D. Schnurr, J. Taylor, T. Luhman,  
617 E. Luhman, C. Ng, R. Wang, and A. Ramesh. Video generation models as world simulators. 2024.  
618 URL <https://openai.com/research/video-generation-models-as-world-simulators>.

619 R. T. Q. Chen, Y. Rubanova, J. Bettencourt, and D. Duvenaud. Neural ordinary differential equations.  
620 *Neural Information Processing Systems (NeurIPS)*, 2018.

621 R. T. Q. Chen, J. Behrmann, D. Duvenaud, and J.-H. Jacobsen. Residual flows for invertible generative  
622 modeling, 2020. URL <https://arxiv.org/abs/1906.02735>.

623 L. Dinh, D. Krueger, and Y. Bengio. Nice: Non-linear independent components estimation. *arXiv  
624 preprint arXiv:1410.8516*, 2014.

625 L. Dinh, J. Sohl-Dickstein, and S. Bengio. Density estimation using real nvp. *arXiv preprint  
626 arXiv:1605.08803*, 2016.

627 C. Durkan, A. Bekasov, I. Murray, and G. Papamakarios. Neural spline flows. *Advances in neural  
628 information processing systems*, 32, 2019.

629 C. Etmann, R. Ke, and C.-B. Schönlieb. iunets: Fully invertible u-nets with learnable up- and  
630 downsampling, 2020. URL <https://arxiv.org/abs/2005.05220>.

631 K. Frans, D. Hafner, S. Levine, and P. Abbeel. One step diffusion via shortcut models. *arXiv preprint  
632 arXiv:2410.12557*, 2024.

633 T. Geffner, K. Didi, Z. Zhang, D. Reidenbach, Z. Cao, J. Yim, M. Geiger, C. Dallago, E. Kucukbenli,  
634 A. Vahdat, et al. Proteina: Scaling flow-based protein structure generative models. *arXiv preprint  
635 arXiv:2503.00710*, 2025.

636 Z. Geng, A. Pokle, W. Luo, J. Lin, and J. Z. Kolter. Consistency models made easy, 2024. URL  
637 <https://arxiv.org/abs/2406.14548>.

648 Z. Geng, M. Deng, X. Bai, J. Z. Kolter, and K. He. Mean flows for one-step generative modeling,  
 649 2025. URL <https://arxiv.org/abs/2505.13447>.

650

651 D. Ghamari, P. Hauke, R. Covino, and P. Faccioli. Sampling rare conformational transitions with a  
 652 quantum computer. *Scientific Reports*, 12(1):16336, 2022.

653 E. Hairer, S. P. Nørsett, and G. Wanner. *Solving Ordinary Differential Equations I: Nonstiff Problems*,  
 654 volume 8 of *Springer Series in Computational Mathematics*. Springer-Verlag, 2nd edition, 1993.  
 655 ISBN 978-3-540-56670-0.

656

657 K. He, X. Zhang, S. Ren, and J. Sun. Deep residual learning for image recognition, 2015. URL  
 658 <https://arxiv.org/abs/1512.03385>.

659

660 J. Heek, E. Hoogeboom, and T. Salimans. Multistep consistency models, 2024. URL <https://arxiv.org/abs/2403.06807>.

661

662 J. Ho, A. Jain, and P. Abbeel. Denoising diffusion probabilistic models, 2020. URL <https://arxiv.org/abs/2006.11239>.

663

664 G. Huguet, J. Vuckovic, K. Fatras, E. Thibodeau-Laufer, P. Lemos, R. Islam, C.-H. Liu, J. Rector-  
 665 Brooks, T. Akhoud-Sadegh, M. Bronstein, et al. Sequence-augmented se (3)-flow matching for  
 666 conditional protein backbone generation. *arXiv preprint arXiv:2405.20313*, 2024.

667

668 K.-H. Hui, C. Liu, X. Zeng, C.-W. Fu, and A. Vahdat. Not-so-optimal transport flows for 3d point  
 669 cloud generation. In *ICLR*, 2025.

670

671 M. F. Hutchinson. A stochastic estimator of the trace of the influence matrix for laplacian smoothing  
 672 splines. *Communications in Statistics-Simulation and Computation*, 18(3):1059–1076, 1989.

673

674 I. Ishikawa, T. Teshima, K. Tojo, K. Oono, M. Ikeda, and M. Sugiyama. Universal approximation  
 675 property of invertible neural networks. *Journal of Machine Learning Research*, 24(287):1–68,  
 676 2023.

677

678 D. Kim, C.-H. Lai, W.-H. Liao, N. Murata, Y. Takida, T. Uesaka, Y. He, Y. Mitsufuji, and S. Ermon.  
 679 Consistency trajectory models: Learning probability flow ode trajectory of diffusion, 2024. URL  
 680 <https://arxiv.org/abs/2310.02279>.

681

682 D. P. Kingma and P. Dhariwal. Glow: Generative flow with invertible 1x1 convolutions, 2018. URL  
 683 <https://arxiv.org/abs/1807.03039>.

684

685 L. Klein, A. Krämer, and F. Noé. Equivariant flow matching. *Advances in Neural Information  
 686 Processing Systems*, 36:59886–59910, 2023.

687

688 A. Kolesnikov, A. S. Pinto, and M. Tschannen. Jet: A modern transformer-based normalizing flow.  
 689 *arXiv preprint arXiv:2412.15129*, 2024.

690

691 Z. Kong and K. Chaudhuri. Universal approximation of residual flows in maximum mean discrepancy.  
 692 *arXiv preprint arXiv:2103.05793*, 2021.

693

694 Y. Lipman, R. T. Q. Chen, H. Ben-Hamu, M. Nickel, and M. Le. Flow matching for generative  
 695 modeling. *International Conference on Learning Representations (ICLR)*, 2023.

696

697 J. S. Liu. *Monte Carlo Strategies in Scientific Computing*. Springer, 2001.

698

699 Q. Liu. Rectified flow: A marginal preserving approach to optimal transport. *arXiv preprint  
 700 arXiv:2209.14577*, 2022.

701

702 X. Liu, C. Gong, and Q. Liu. Flow straight and fast: Learning to generate and transfer data with  
 703 rectified flow. *International Conference on Learning Representations (ICLR)*, 2023.

704

705 C. Lu and Y. Song. Simplifying, stabilizing and scaling continuous-time consistency models. *arXiv  
 706 preprint arXiv:2410.11081*, 2024.

707

708 S. Moqvist, W. Chen, M. Schreiner, F. Nuske, and S. Olsson. Thermodynamic interpolation: A  
 709 generative approach to molecular thermodynamics and kinetics. *Journal of Chemical Theory and  
 710 Computation*, 21(5):2535–2545, 2025.

702 F. Noé, S. Olsson, J. Köhler, and H. Wu. Boltzmann generators: Sampling equilibrium states of  
 703 many-body systems with deep learning. *Science*, 365(6457):eaaw1147, 2019.

704

705 G. Papamakarios, E. Nalisnick, D. J. Rezende, S. Mohamed, and B. Lakshminarayanan. Normalizing  
 706 flows for probabilistic modeling and inference. *Journal of Machine Learning Research*, 22(57):  
 707 1–64, 2021.

708 S. Peluchetti. Non-denoising forward-time diffusions. *arXiv preprint arXiv:2312.14589*, 2023.

709

710 G. Peyré and M. Cuturi. Computational optimal transport. *Foundations and Trends in Machine  
 711 Learning*, 11(5-6):355–607, 2019.

712 D. Rezende and S. Mohamed. Variational inference with normalizing flows. In *International  
 713 conference on machine learning*, pages 1530–1538. PMLR, 2015.

714

715 A. Rizzi, P. Carloni, and M. Parrinello. Targeted free energy perturbation revisited: Accurate free  
 716 energies from mapped reference potentials. *The journal of physical chemistry letters*, 12(39):  
 717 9449–9454, 2021.

718 A. Sabour, S. Fidler, and K. Kreis. Align your flow: Scaling continuous-time flow map distillation,  
 719 2025. URL <https://arxiv.org/abs/2506.14603>.

720 A. Sauer, D. Lorenz, A. Blattmann, and R. Rombach. Adversarial diffusion distillation. In *European  
 721 Conference on Computer Vision*, pages 87–103. Springer, 2024.

722

723 J. Song, C. Meng, and S. Ermon. Denoising diffusion implicit models, 2022. URL <https://arxiv.org/abs/2010.02502>.

724

725 Y. Song and P. Dhariwal. Improved techniques for training consistency models, 2023. URL <https://arxiv.org/abs/2310.14189>.

726

727 Y. Song, P. Dhariwal, M. Chen, and I. Sutskever. Consistency models, 2023. URL <https://arxiv.org/abs/2303.01469>.

728

729 E. G. Tabak and C. V. Turner. A family of nonparametric density estimation algorithms. *Communications on Pure and Applied Mathematics*, 66(2):145–164, 2013.

730

731 E. G. Tabak and E. Vanden-Eijnden. Density estimation by dual ascent of the log-likelihood. *Communications in Mathematical Sciences*, 2010.

732

733 C. B. Tan, A. J. Bose, C. Lin, L. Klein, M. M. Bronstein, and A. Tong. Scalable equilibrium sampling  
 734 with sequential boltzmann generators. *arXiv preprint arXiv:2502.18462*, 2025a.

735

736 C. B. Tan, M. Hassan, L. Klein, S. Syed, D. Beaini, M. M. Bronstein, A. Tong, and K. Neklyudov.  
 737 Amortized sampling with transferable normalizing flows. *arXiv preprint arXiv:2508.18175*, 2025b.

738

739 T. Teshima, I. Ishikawa, K. Tojo, K. Oono, M. Ikeda, and M. Sugiyama. Coupling-based invertible  
 740 neural networks are universal diffeomorphism approximators. *Advances in Neural Information  
 741 Processing Systems*, 33:3362–3373, 2020.

742

743 A. Tong, N. Malkin, G. Huguet, Y. Zhang, J. Rector-Brooks, K. Fatras, G. Wolf, and Y. Bengio.  
 744 Improving and generalizing flow-based generative models with minibatch optimal transport. *arXiv  
 745 preprint arXiv:2302.00482*, 2023.

746

747 C. Villani. *Topics in optimal transportation*, volume 58. American Mathematical Soc., 2021.

748

749 P. Wirnsberger, A. J. Ballard, G. Papamakarios, S. Abercrombie, S. Racanière, A. Pritzel,  
 750 D. Jimenez Rezende, and C. Blundell. Targeted free energy estimation via learned mappings. *The  
 751 Journal of Chemical Physics*, 153(14), 2020.

752

753 Z. Xu and T. Campbell. Embracing the chaos: analysis and diagnosis of numerical instability in  
 754 variational flows. *Advances in Neural Information Processing Systems*, 36:32360–32386, 2023.

755

T. Yin, M. Gharbi, R. Zhang, E. Shechtman, F. Durand, W. T. Freeman, and T. Park. One-step  
 756 diffusion with distribution matching distillation. In *Proceedings of the IEEE/CVF conference on  
 757 computer vision and pattern recognition*, pages 6613–6623, 2024.

756 S. Zhai, R. Zhang, P. Nakkiran, D. Berthelot, J. Gu, H. Zheng, T. Chen, M. A. Bautista, N. Jaitly, and  
757 J. Susskind. Normalizing flows are capable generative models. *arXiv preprint arXiv:2412.06329*,  
758 2024.

759 H. Zhang, X. Gao, J. Unterman, and T. Arodz. Approximation capabilities of neural odes and  
760 invertible residual networks. In *International Conference on Machine Learning*, pages 11086–  
761 11095. PMLR, 2020.

762 L. Zhou, S. Ermon, and J. Song. Inductive moment matching. *arXiv preprint arXiv:2503.07565*,  
763 2025.

764 M. Zhou, H. Zheng, Z. Wang, M. Yin, and H. Huang. Score identity distillation: Exponentially fast  
765 distillation of pretrained diffusion models for one-step generation. In *Forty-first International  
766 Conference on Machine Learning*, 2024.

767 R. W. Zwanzig. High-temperature equation of state by a perturbation method. i. nonpolar gases.  
768 *The Journal of Chemical Physics*, 22(8):1420–1426, 08 1954. ISSN 0021-9606. doi: 10.1063/1.  
769 1740409. URL <https://doi.org/10.1063/1.1740409>.

770

771

772

773

774

775

776

777

778

779

780

781

782

783

784

785

786

787

788

789

790

791

792

793

794

795

796

797

798

799

800

801

802

803

804

805

806

807

808

809

## 810 A PROOFS

## 811 A.1 PROOF OF PROPOSITION 1

812 We first recall proposition 1 below.

813 **Proposition 1.** Suppose that  $f_t^*$  is invertible for all  $t$ , that  $(f_t^*)^{-1}$  is continuous for all  $t$ . Then,  
814 as  $\mathcal{L}(\theta) \rightarrow 0$ , it holds that  $((f_t^*)^{-1} \circ f_{t,\theta})(x) \rightarrow x$  for almost all (with respect to  $p_0$ )  $x$ .815 To prove proposition 1, we first prove the following lemma, which is essentially the same as the  
816 proposition, but it abstracts out the distribution of  $x_t$ , which depends on  $x_0$ ,  $x_1$ , and  $t$ .817 **Lemma 1.** For functions  $(f_n)_{n \geq 1}$  and  $g$ , where  $g$  is invertible and has a continuous inverse,  
818  $x_0 \sim p_0$ , if  $\text{MSE}(f_n, g) := \mathbb{E}_{x_0} \|f_n(x_0) - g(x_0)\|_2^2 \rightarrow 0$ , then  $\lim_{n \rightarrow \infty} g^{-1}(f_n(x)) = x$  for  
819 almost all (with respect to  $p_0$ )  $x$ .820 *Proof.* Let  $Y_n = \|f_n(x_0) - g(x_0)\|_2$ . We know that  $\lim_{n \rightarrow \infty} \mathbb{E}[Y_n^2] = 0$  (as it corresponds to the  
821 MSE), which implies that  $\lim_{n \rightarrow \infty} \text{Var}(Y_n) = 0$ . Consequently,  $Y_n \rightarrow c$  for some constant  $c \in \mathbb{R}$ .  
822 Moreover, by Jensen's inequality and the convexity of  $x \mapsto x^2$ , we find that  $(\mathbb{E}[Y_n])^2 \leq \mathbb{E}[Y_n^2]$ ,  
823 meaning that  $c = 0$ . This implies that  $\lim_{n \rightarrow \infty} \|f_n(x) - g(x)\|_2^2 = 0$  almost everywhere, and thus  
824 that  $\lim_{n \rightarrow \infty} f_n(x) = g(x)$ . Finally, since  $g^{-1}$  is continuous, we can apply the function to both sides  
825 of the limit to find that  $\lim_{n \rightarrow \infty} g^{-1}(f_n(x)) = x$ , almost everywhere.  $\square$ 826 It suffices to apply the above lemma to  $x_t \sim p_t(\cdot | x_0, x_1) p_1(x_1 | x_0) p_0(x_0)$ .

## 827 A.2 PROOF OF PROPOSITION 2

828 We now prove proposition 2. The proposition reuses the following regularity assumptions, as  
829 introduced in Benton et al. (2023), which we recall verbatim below for convenience:830 **(Assumption 1)** Let  $v_{\text{true}}$  be the true generating velocity field for the CNF with field  $v^*$  trained using  
831 flow matching. Then the true and learned velocity  $v^*$  are close in  $\ell_2$  and satisfy:

832 
$$\int_0^1 \mathbb{E}_{t,x_t} [\|v_{t,\text{true}}(x_t) - v_t^*(x_t)\|^2] dt \leq K^2.$$

833 **(Assumption 2)** For each  $x \in \mathbb{R}^d$  and  $s \in [0, 1]$ , there exists unique flows  $(f_{s,t}^*)_{t \in [s,1]}$  and  
834  $(f_{s,t})_{t \in [s,1]}$ , starting at  $f_{(s,s)}^* = x$  and  $f_{(s,s),\text{true}} = x$  with velocity fields  
835  $v_t^*(x_t)$  and  $v_{t,\text{true}}(x_t)$ , respectively. Additionally,  $f^*$  and  $f_{\text{true}}$  are continuously  
836 differentiable in  $x$ ,  $s$  and  $t$ .837 **(Assumption 3)** The velocity field  $v_t^*(x_t)$  is differentiable in both  $x$  and  $t$ , and also for each  $t \in [0, 1]$   
838 there exists a constant  $L_t$  such that  $v_t^*(x_t)$  is  $L_t$ -Lipschitz in  $x$ .839 **Proposition 2.** Let  $p_{\text{reflow}}$  be a pretrained CNF generated by the vector field  $v_t^*$ , real numbers  
840  $(L_t)_{t \in [0,1]}$  such that  $v_t^*$  is  $L_t$ -Lipschitz for all  $t \in [0, 1]$ , and a NF  $f_\theta^{\text{nf}}$  trained using Eq. 5 by  
841 regressing against  $f_{\text{reflow}}^*(x_0)$ , where  $x_0 \sim \mathcal{N}(0, I)$ . Then, writing  $p_\theta^{\text{nf}} := \text{Law}(f_\theta^{\text{nf}}(x_0))$ , we have:

842 
$$\mathcal{W}_2(p_1, p_\theta) \leq K \exp \left( \int_0^1 L_t dt \right) + \epsilon, \quad K \geq \int_0^1 \mathbb{E} [\|v_t^*(x_t) - v_{t,\text{true}}(x_t)\|_2^2]^{1/2} dt, \quad (10)$$

843 where  $K$  is the  $\ell_2$  approximation error between the velocity field of the CNF and the ground  
844 truth generating field  $v_t^*$ ,  $\epsilon^2 = \mathbb{E}_{x_0,x_1} [\|f_{\text{reflow}}^*(x_0) - f_\theta^{\text{nf}}(x_0)\|_2^2]$ .845 *Proof.* We begin by first applying the triangle inequality to  $\mathcal{W}_2(p_1, p_\theta)$  and obtain:

846 
$$\mathcal{W}_2(p_1, p_\theta) \leq \mathcal{W}_2(p_1, p_{\text{reflow}}) + \mathcal{W}_2(p_{\text{reflow}}, p_\theta^{\text{nf}}). \quad (11)$$

847 The first term is an error in Wasserstein-2 distance between the true data distribution and our reflow  
848 targets, which is still a CNF. A straightforward application of Theorem 1 in Benton et al. (2023)  
849 gives a bound on this first Wasserstein-2 distance<sup>1</sup>:

850 
$$\mathcal{W}_2(p_1, p_{\text{reflow}}) \leq K \exp \left( \int_0^1 L_t dt \right). \quad (12)$$

851 <sup>1</sup>A sharper bound can be obtained with additional assumptions, as demonstrated in Benton et al. (2023), but  
852 it is not critically important in our context.

To bound  $\mathcal{W}_2(p_{\text{reflow}}, p_\theta)$ , recall that the following inequality holds  $\mathcal{W}_2(\text{Law}(X), \text{Law}(Y)) \leq \mathbb{E} [\|X - Y\|_2^2]^{\frac{1}{2}}$ , for any two random variables  $X$  and  $Y$ . In our case, these random variables are  $p_{\text{reflow}}^* = \text{Law}(f_{\text{reflow}}^*(x_0))$  and  $p_\theta^{\text{nf}} = \text{Law}(f_\theta^{\text{nf}}(x_0))$ . This gives:

$$\mathcal{W}_2(p_{\text{reflow}}, p_\theta^{\text{nf}}) \leq \mathbb{E}_{x_0, x_1} \left[ \|f_{\text{reflow}}^*(x_0) - f_\theta^{\text{nf}}(x_0)\|_2^2 \right]^{\frac{1}{2}}. \quad (13)$$

Combining eq. (12) and eq. (13) achieves the desired result and completes the proof.  $\square$

$$\mathcal{W}_2(p_1, p_\theta) \leq K \exp \left( \int_0^1 L_t dt \right) + \mathbb{E}_{x_0, x_1} \left[ \|f_{\text{reflow}}^*(x_0) - f_\theta^{\text{nf}}(x_0)\|_2^2 \right]^{\frac{1}{2}}. \quad (14)$$

Note that the bound on  $\mathcal{W}_2(p_{\text{reflow}}, p_\theta^{\text{nf}})$  is effectively the square-root of the REGFLOW objective and thus optimization of the NF using this loss directly minimizes the upper bound to  $\mathcal{W}_2(p_1, p_\theta^{\text{nf}})$ .

### A.3 REGFLOW IN CONTINUOUS TIME

Current state-of-the-art CNFs are trained using “flow matching” (Lipman et al., 2023; Albergo and Vanden-Eijnden, 2023; Liu et al., 2023), which attempts to match the vector field associated with the flow to a target vector field that solves for mass transportation everywhere in space and time. Specifically, we can cast conditional flow matching (CFM) (Tong et al., 2023) from the perspective of REGFLOW. To see this explicitly, consider a pre-specified probability path,  $p_t(x_t)$ , and the following  $f_{t, \text{fm}}^* = \frac{\partial}{\partial t} p_t(x_t)$ . However, since it is generally computationally challenging to sample from  $p_t$  directly, the marginalization trick is used to derive an equivalent objective with a conditional  $f_{t, \text{cfm}}^*$ . We note that REGFLOW requires  $f_{t, \text{cfm}}^*$  to be invertible therefore this assumes regularity on  $\frac{\partial}{\partial t} p_t(x_t)$ . This is generally satisfied by adding a small amount of noise to the following. We present this simplified form for clarity.

$$p_t(x_t) := \int p_t(x_t | x_0, x_1) d\pi(x_0, x_1), \quad p_t(x_t | x_0, x_1) = \delta(x_t; (1-t)x_0 + tx_1). \quad (15)$$

Then setting  $f_{t, \text{cfm}}^* = \frac{\partial}{\partial t} p_t(x_t | x_0, x_1)$  it is easy to show that:

$$\begin{aligned} \mathcal{L}(\theta) &= \mathbb{E}_{t, x_0, x_1, x_t} \left[ \left\| v_{t, \theta}(x_t) - \frac{\partial}{\partial t} p_t(x_t | x_0, x_1) \right\|^2 \right] = \mathbb{E}_{t, x_t} \left[ \left\| v_{t, \theta}(x_t) - \frac{\partial}{\partial t} p_t(x_t) \right\|^2 \right] + C, \\ &= \mathbb{E}_{t, x_0, x_1, x_t} \left[ \lambda_t \|f_{t, \theta}(x_t) - f_{t, \text{cfm}}^*(x_t)\|^2 \right], \end{aligned}$$

with  $C$  independent of  $\theta$  (Lipman et al., 2023), and  $\lambda_t$  is a loss weighting, which fits within the REGFLOW framework in the continuous-time setting with the last equality known as target/end-point prediction.

### A.4 REQUIREMENTS FOR REGFLOW TARGETS

In practice, REGFLOW deals with discrete couplings. Any discrete coupling is usable for training RegFlow as long as there exists an invertible function on the continuous domain which agrees with it. This leaves us with easily verifiable necessary and sufficient properties for the base coupling. Specifically, let  $\pi(x_0, x_1)$  denote the coupling between empirical point sets  $x_0, x_1$  in  $\mathbb{R}^d$ .

**Proposition 3.** *If  $\pi$  is a permutation and there does not exist  $i \neq j$  such that  $x_0^i = x_0^j$  or  $x_1^i = x_1^j$ . Then there exists invertible function  $f : \mathbb{R}^d \rightarrow \mathbb{R}^d$  such that for all  $x_0^i \in x_0$ ,  $f(x_0^i) = x_1^i$  and for all  $x_1^i \in x_1$ ,  $f^{-1}(x_1^i) = x_0^i$ .*

*Proof.* We proceed by constructing an example  $f$  which satisfies the necessary properties. First we denote  $f^* : x_0 \rightarrow x_1$  as the discrete invertible function mapping the point set  $x_0$  to the point set  $x_1$ . Let

$$f(x) = \begin{cases} f^*(x) & \text{if } x \in x_0 \\ f^{*-1}(x) & \text{if } x \in x_1 \\ x & \text{else} \end{cases}$$

This function is invertible on  $\mathbb{R}^d$  and satisfies the necessary properties in the proposition on the domains of  $x_0$  and  $x_1$ .  $\square$

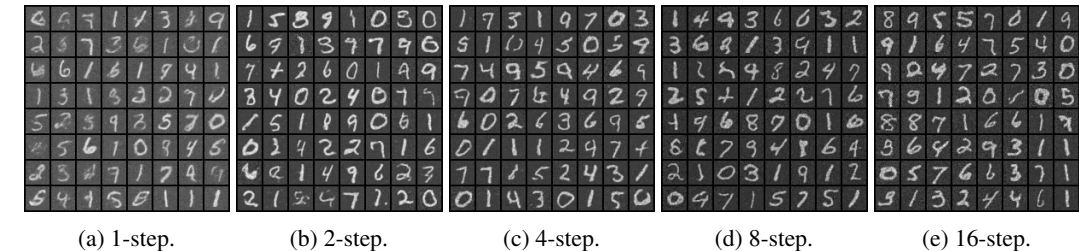


Figure 6: Generations of IMM trained with an iUNet with a variable number of steps.

This proposition establishes necessary and sufficient conditions for training a valid REGFLOW between  $x_0$  and  $x_1$ . This property is quite simple to obtain in practice. For both OT-couplings and CNF-couplings  $\pi$  is almost by definition a permutation. The only trouble is if there exist duplicate points. This is a measure-zero event in continuous space, and therefore is not an issue.

In fact, any random permutation matrix satisfies these conditions. Which leads to the perhaps more interesting question of what are the properties of a “good” coupling  $\pi$ . In some sense we are looking for  $\pi$  that are “good” couplings that are somehow “easy” to learn and generalizes well when trained with the REGFLOW procedure in a given setting.

In this work we used REGFLOW to improve the training speed and convergence of the same normalizing flow architectures that are normally trained using maximum likelihood (MLE).

We believe the classic MLE objective would help when it is difficult to find a good coupling for the given architecture, dataset, and REGFLOW learning framework. In this work we established that there exist settings where OT and CNF-couplings outperform the MLE objective. We leave it to future work to study the optimal couplings in a given setting.

## B ADDITIONAL BACKGROUND

## B.1 INDUCTIVE MOMENT MATCHING

Introduced in Zhou et al. (2025), Inductive Moment Matching (IMM) defines a training procedure for one-step generative models, based on diffusion/flow matching. Specifically, IMM trains models to minimize the difference in distribution between different points in time induced by the model. As a result, this avoids direct optimization for the predicted endpoint, in contrast to conventional diffusion. More precisely, let  $f_\theta : \mathbb{R}^d \times [0, 1]^2 \rightarrow \mathbb{R}^d$ ,  $(x, s, t) \mapsto f_\theta(x, s, t)$  be a function parameterized by  $\theta$ . IMM minimizes the following maximum mean discrepancy (MMD) loss:

$$\mathcal{L}(\theta_n) = \mathbb{E}_{s,t,x_0,x_1} \left[ w(s,t) \text{MMD}^2 \left( p_{\theta_{n-1},(s|r)}(x_s), p_{\theta_n,(s|t)}(x_s) \right) \right], \quad (16)$$

where  $0 \leq r \leq r(s, t) := r \leq s \leq 1$ , with  $s, t \sim \mathcal{U}(0, 1)$  iid,  $w \geq 0$  is a weighting function,  $x_1$  is a sample from the target distribution,  $x_0 \sim \mathcal{N}(0, I)$ ,  $x_s$  is some interpolation between  $x_0$  and  $x_1$  at time  $s$  (typically, using the DDIM interpolation (Song et al., 2022)), the subscript  $n \in \mathbb{N}$  of parameter  $\theta$  refers to its training step, and MMD is some MMD function based on a chosen kernel (typically, Laplace).<sup>2</sup> Essentially, the method uses as a target the learned distribution of the previous step at a higher time to train the current distribution at lower times. With a skip parameterization, the higher time distribution is by construction close to the true solution, as  $p_\theta(x_s \mid x_r) \approx p(x_s \mid x_r)$  when  $r \approx s$ , and  $x_s$  is known. (Or, in other terms,  $f_\theta(x, s, r \approx s) \approx x$  with the skip parameterization.) When the distributions match (when the loss is zero),  $\text{MMD}^2(p_{1,\theta}, p_1) = 0$ , and so the generative model's and the target distribution's respective moments all match.

This training procedure allows for variable-step sampling. For chosen timesteps,  $(t_i)_{i=1}^n$ , one can sample from  $p_{1|\theta}$  by sampling  $x_0 \sim \mathcal{N}(0, I)$  and performing the steps:

$$x_{t+1} \leftarrow \text{DDIM}(f_\theta(x_t, t_{i+1}, t_i), x_t, t_i, t_{i+1}), \quad (17)$$

where DDIM is the DDIM interpolant



972  
973  
974  
975  
976  
977  
978  
979  
980  
981  
982  
983  
984  
985  
986  
987  
988  
989  
990  
991  
992  
993  
994  
995  
996  
997  
998  
999  
1000  
1001  
1002  
1003  
1004  
1005  
1006  
1007  
1008  
1009  
1010  
1011  
1012  
1013  
1014  
1015  
1016  
1017  
1018  
1019  
1020  
1021  
1022  
1023  
1024  
1025

(a) Using the ResFlow architecture proposed in [Chen et al. \(2020\)](#). (b) Using the TarFlow architecture [\(Zhai et al., 2024\)](#),  $m = 4$ . (c) Using the TarFlow architecture [\(Zhai et al., 2024\)](#),  $m = 16$ .

Figure 7: One-step generation results with a Lipschitz-constrained (ResFlow) model and an invertible model (TarFlow) for IMM. The  $m$  parameter is the group size in IMM used to approximate the MMD.

## B.2 INDUCTIVE MOMENT MATCHING NEGATIVE RESULTS

We detail in appendix B.1 the Inductive Moment Matching (IMM) framework [\(Zhou et al., 2025\)](#). Observing the sampling procedure, which we give in eq. (17), one can make this procedure invertible by constraining the Lipschitz constant of the model, or by using an invertible model. For the first case, if we use the “Euler” (skip) parameterization alongside the DDIM interpolation, it is shown that the reparameterized model  $g_\theta$  can be written as:

$$\forall x, s, t, \quad g_\theta(x, s, t) = x - (s - t)f_\theta(x, s, t). \quad (18)$$

Moreover,  $0 \leq s - t \leq 1$ , and so if the Lipschitz constant of  $f_\theta$  is strictly less than one, then the overall model is invertible, using the argument of residual flows [\(Behrmann et al., 2019\)](#); so the change of variables formula applies as follows (using the time notation of IMM/diffusion):

$$\log p_1^\theta(x) = \log p_0(x_0) - \sum_i \log \left[ (t_{i+1} - t_i) \det(J_{f_\theta(\cdot, t_{i+1}, t_i)}(x_{t_i})) \right], \quad (19)$$

The difficulty of evaluating the log-determinant of the Jacobian remains. Note, however, that we do not need to find the inverse of the function to evaluate the likelihood of generated samples, since we know each  $(x_{t_i})_i$ . The second path (of using an invertible model) is viable only for one-step sampling with no skip parameterization (which, according to [Zhou et al. \(2025\)](#), tends to under-perform, empirically), since the sampling procedure then boils down to  $x_1 = f(x_0, 1, 0)$  for  $x_0 \sim \mathcal{N}(0, I)$ .

While both approaches succeeded in synthetic experiments, they fail to scale to datasets such as MNIST, the results of which we include here in fig. 6 and in fig. 7. We have tried iUNet [\(Etmann et al., 2020\)](#) and TarFlow [\(Zhai et al., 2024\)](#), an invertible UNet and a Transformer-based normalizing flow, respectively, for invertible one-step models; and we have tried the ResFlow architecture in [\(Chen et al., 2020\)](#) for the Lipschitz-constrained approach. As observed, TarFlow fails to produce images of high quality; iUNets produced significantly better results, albeit still not sufficient, especially for the one-step sampling, which is the only configuration that guarantees invertibility; the Lipschitz-constrained ResFlow entirely failed to produce satisfactory results, although the loss did diminish during training. In general, an even more important limitation is the difficulty of designing invertible or Lipschitz-constrained models for other data types, for instance, 3D coordinates. Perhaps further research on the architectural side could allow for higher performance with invertible sampling.

## C EXPERIMENTAL DETAILS

### C.1 METRICS

The performance metrics considered across the investigated flows were the effective sample size, ESS, Wasserstein-1 energy distance,  $\mathcal{E}\mathcal{W}_1$ , and the Wasserstein-2 distance on dihedral angles,  $\mathbb{T}\mathcal{W}_2$ .

<sup>2</sup>Note that we have adapted IMM’s notation to our time notation, with noise at time zero, and clean data at time one.

1026  
1027 **Effective Sample Size (ESS).** We compute the effective sample size (ESS) using Kish’s formula,  
1028 normalized by the number of samples generated:

1029 
$$\text{ESS}(\{w_i\}_{i=1}^N) = \frac{1}{N} \frac{\left(\sum_{i=1}^N w_i\right)^2}{\sum_{i=1}^N w_i^2}. \quad (20)$$
  
1030  
1031

1032 where  $w_i$  is the unnormalized weight of each particle indexed by  $i$  over  $N$  particles. Effective sample  
1033 size measures the variance of the weights and approximately how many more samples would be  
1034 needed compared to an unbiased sample. For us, this captures the local quality of the proposal relative  
1035 to the ground truth energy. It does not rely on a ground truth test set; however, it is quite sensitive  
1036 and may be misleading in the case of dropped modes or incomplete coverage, as it only measures  
1037 agreement on the support of the generated distribution.

1038 **Wasserstein-1 Energy Distance ( $\mathcal{E}\text{-}\mathcal{W}_1$ ).** The Wasserstein-1 energy distance measures how well  
1039 the generated distribution matches some ground truth sample (often generated using MD data) by  
1040 calculating the Wasserstein-1 distance between the energy histograms. Specifically:

1041 
$$\mathcal{E}\text{-}\mathcal{W}_1(x, y) = \min_{\pi} \int_{x, y} |x - y| d\pi(x, y), \quad (21)$$
  
1042

1043 where  $\pi$  is a valid coupling of  $p(x)$  and  $p(y)$ . For discrete distributions of equal size,  $\pi$  can be thought  
1044 of as a permutation matrix. This measures the model’s ability to generate very accurate structures  
1045 as the energy function we use requires extremely accurate bond lengths to obtain reasonable energy  
1046 values. When the bond lengths have minor inaccuracies, the energy can blow up extremely quickly.

1047 **Torus Wasserstein ( $\mathbb{T}\text{-}\mathcal{W}_2$ ).** The torus Wasserstein distance measures the Wasserstein-2 dis-  
1048 tance on the torus defined by the main torsion angles of the peptide. That is for a peptide of  
1049 length  $l$ , there are  $2(l - 1)$  torsion angles defining the *dihedrals* along the backbone of interest  
1050 ( $(\phi_1, \psi_1), (\phi_2, \psi_2), \dots (\phi_l, \psi_l)$ ). We define the torus Wasserstein distance over these backbone  
1051 angles as:

1052 
$$\mathbb{T}\text{-}\mathcal{W}_2(p, q)^2 = \min_{\pi} \int_{x, y} c_{\mathcal{T}}(x, y)^2 d\pi(x, y), \quad (22)$$
  
1053

1054 where  $\pi$  is a valid coupling between  $p$  and  $q$ , and  $c_{\mathcal{T}}(x, y)^2$  is the shortest distance on the torus  
1055 defined by the dihedral angles:

1056 
$$c_{\mathcal{T}}(x, y)^2 = \sum_{i=0}^{2(L-1)} [(\text{Dihedrals}(x)_i - \text{Dihedrals}(y)_i + \pi) \bmod 2\pi - \pi]^2. \quad (23)$$
  
1057  
1058

1059 The torus Wasserstein distance measures large scale changes and is quite important for understanding  
1060 mode coverage and overall macro distribution. We find REGFLOW does quite well in this regard.

## 1062 C.2 ADDITIONAL DETAILS ON EXPERIMENTAL SETUP

1064 To accurately compute the previously defined metrics, 250k proposal samples were drawn and  
1065 re-weighted for alanine dipeptide, tripeptide, and tetrapeptide.

1066 **Data normalization.** We adopt the same data normalization strategy proposed in (Tan et al., 2025a),  
1067 in which the center of mass of each atom is first subtracted from the data, followed by scaling using  
1068 the standard deviation of the training set.

1069 **Exponential moving average.** We apply an exponential moving average (EMA) on the weights of all  
1070 models, with a decay of 0.999, as commonly done in flow-based approaches to improve performance.

1072 **Training details and hardware.** All models were trained on NVIDIA L40S 48GB GPUs for 5000 epochs, except those using  
1073 OT targets, which were trained for 2000 epochs. Convergence was  
1074 noted earlier in the OT experiments, leading to early stopping. The  
1075 total training time for all models is summarized in table 7. The time  
1076 taken to compute the OT map is also provided; since computing the  
1077 OT map is independent of the feature dimension, but only on the  
1078 number of data points used, the compute time was relatively consistent  
1079 across all datasets. A total of 100k points was used for training  
the CNF, performing MLE training, and computing the OT map.

1072 Table 7: REGFLOW training time  
1073 (in hours) on ALDP, AL3, and  
1074 AL4.

Model	ALDP	AL3	AL4
OT map	3.6	3.8	3.8
DiT CNF	27.6	40.7	48.6
NSF	21.0	23.8	26.8
Res-NVP	15.7	15.6	15.0
Jet	19.1	19.2	20.1

1080  
 1081 **Reflow targets.** Ablations were done to investigate the influence of synthetic data quantity on all  
 1082 metrics. For all benchmarking performed against MLE training, the largest amount of synthetic data  
 1083 was used. For ALDP, AL3, and AL4, this constituted 10.4M, 10.4M, and 10M samples, respectively.

1084 **Determinant regularization.** During REGFLOW, it was initially ob-  
 1085 served that as proposal sample quality improved, the re-weighted sam-  
 1086 ples progressively deteriorated across all metrics due to the models  
 1087 becoming numerically non-invertible. This was partially addressed  
 1088 by adding regularization to the loss in the form of a log deter-  
 1089 minant penalty. Sweeps were conducted using multiple regularization  
 1090 weights ranging between  $10^{-7}$  and  $10^{-4}$  to prevent hampering sam-  
 1091 ple performance. The amount of regularization added was a function  
 1092 of the flow and dataset. The final weights are summarized in table 8.

1093 **Target noise.** To discourage numerical non-invertibility of the trained flows, Guassian noise was  
 1094 also introduced to the target samples. Experiments were conducted with noise magnitudes of 0.01,  
 1095 0.05, 0.1, and 0.25, with a final value of 0.05 being selected for use across models and datasets.

1096 **REGFLOW implementation details.** A summary of all trained model configurations is provided  
 1097 in table 9. To maintain a fair comparison, the configurations reported below were unchanged for  
 1098 MLE training and REGFLOW. Adam was used as the optimizer with a learning rate of  $5 \times 10^{-4}$   
 1099 and a weight decay of 0.01. We also included a varying cosine schedule with warmup in line with  
 the approach suggested in (Tan et al., 2025a).

1100

1101 Table 9: Model configurations for the DiT CNF, NSF, Res–NVP, and Jet across all datasets (ALDP, AL3, AL4).  
 1102 A dash (–) indicates the parameter is not applicable to the respective model.

1103

Model	hidden features	transforms	layers	blocks per layer	conditioning dim.	heads	dropout	# parameters (M)
DiT CNF	768	–	6	–	128	12	0.1	46.3
NSF	256	24	–	5	–	–	–	76.8
Res–NVP	512	–	8	6	–	–	0.1	80.6
Jet	432	–	4	12	128	12	0.1	77.6

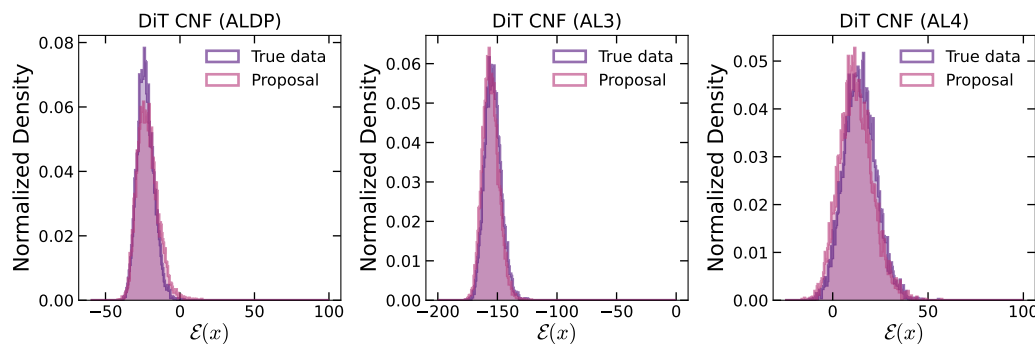
1108

1109

1110 **Quality of CNF targets.** To maximize the likelihood that models trained with REGFLOW have the  
 1111 potential to outperform MLE, securing high-quality targets is essential. In line with this pursuit,  
 1112 a CNF with a diffusion transformer backbone was used. In fig. 8, the true data and the CNF proposal  
 1113 are shown, where it can be seen that the learned energy distributions across all three peptides  
 1114 are nearly perfect. Re-weighted samples are not included as obtaining likelihoods from the CNF  
 1115 requires estimating the trace of the divergence, which is often an expensive operation with a large  
 1116 time and memory cost. Although many unbiased approaches for approximating the likelihood  
 1117 exist (Hutchinson, 1989), these methods are typically unusable for Boltzmann Generators due to  
 1118 their variance, which can introduce bias into the weights needed for importance sampling.

1119

1120



1131 Figure 8: True energy distribution and learned proposal using the DiT-based CNF. \*The re-weighted proposal is  
 1132 not present because it was too computationally expensive to compute for a sufficient number of points.  
 1133

Table 8: Regularization weights used across datasets and flows.

Model	ALDP	AL3	AL4
NSF	$10^{-6}$	$10^{-5}$	$10^{-5}$
Res–NVP	$10^{-5}$	$10^{-5}$	$10^{-6}$
Jet	$10^{-5}$	$10^{-6}$	$10^{-5}$

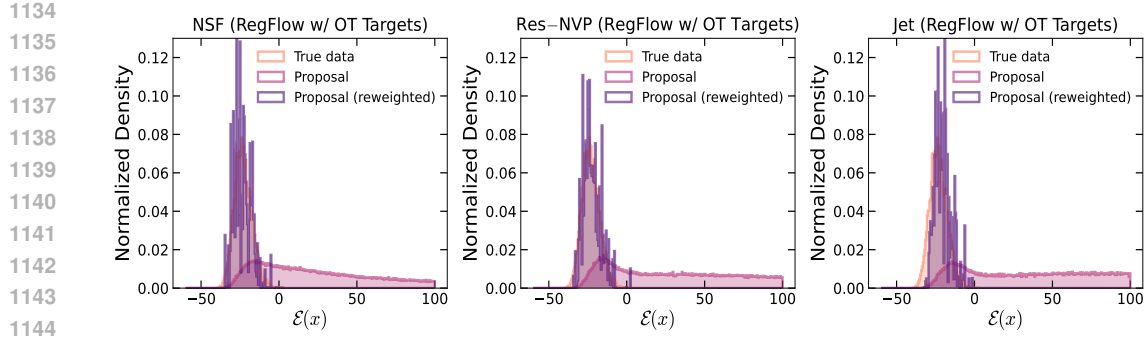


Figure 9: Energy distribution of the original and re-weighted samples, as well as the true data, when using 100,000 OT targets on ALDP (**left**: NSF (REGFLOW); **center**: Res–NVP (REGFLOW); **right**: Jet (REGFLOW)).

## D ADDITIONAL RESULTS

### D.1 REGFLOW PERFORMANCE USING OT TARGETS

**Optimal transport targets.** In addition to using reflow targets from a pre-trained CNF, we pre-compute an OT map to obtain an invertible pairing between source and target samples. We combine this map with REGFLOW training, and report results in fig. 9 for alanine dipeptide. Here, we demonstrate an example of where REGFLOW training goes beyond distillation and can serve as an effective approach at training classical normalizing flows on diverse invertible maps.

### D.2 PERFORMANCE ON LARGER PEPTIDES

**Alanine tripeptide and alanine tetrapeptide** We demonstrate the learned distributions of the two pairs of dihedral angles that parameterize alanine tripeptide and tetrapeptide using our best MLE-trained and REGFLOW flows in fig. 11 and fig. 12. The inability to capture the modes using MLE is elucidated, where multiple modes appear to blend together in both sets of dihedral angles in fig. 11. Conversely, using REGFLOW, most modes are accurately captured and the general form of the Ramachandran plots conforms well to that of the true distribution obtained from MD. The findings observed with alanine tripeptide are even more pronounced with alanine tetrapeptide, where certain modes are entirely missed when MLE-trained flows are used, as seen in fig. 12. With REGFLOW, however, most modes are accurately captured, and the density distribution is in strong agreement with the ground truth data. These findings clearly demonstrate the utility of a regression-based training objective over conventional MLE for applications to equilibrium conformation sampling of peptides.

In fig. 10, we demonstrate that the energy distribution of the re-weighted samples using REGFLOW, which yields a more favourable energy distribution over MLE-trained flows. For the tripeptide, the results are in strong agreement with MD. For the tetrapeptide, the re-weighted samples are superior than their MLE counterparts, but have room for improvement in matching the true energy distribution.

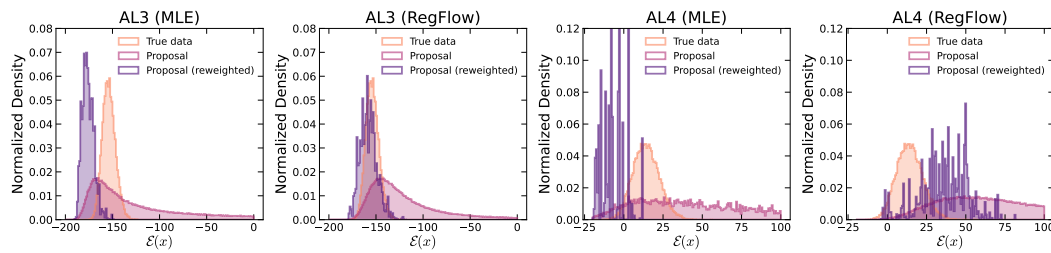


Figure 10: Energy distribution of original and re-weighted samples generated for the most performant MLE and REGFLOW models on alanine tripeptide (**left** and **center left**) and alanine tetrapeptide (**center right** and **right**).

### D.3 GENERATED SAMPLES OF PEPTIDE CONFORMATIONS

**Samples of generated peptides.** Below we provide sample conformations of alanine dipeptide generated using both MLE training and REGFLOW in fig. 13. In addition, we include sample molecules of the larger peptides, obtained through REGFLOW training as well in fig. 14.

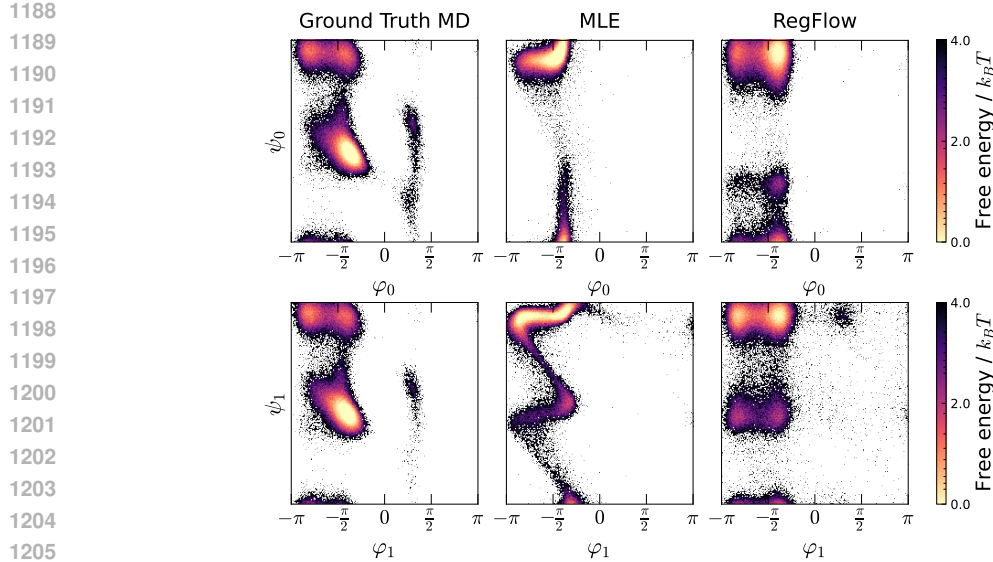


Figure 11: Ramachandran plots for alanine tripeptide (**left**: ground truth, **middle**: best MLE-trained flow, **right**: best REGFLOW flow). REGFLOW captures most modes, while MLE-trained flows struggle.

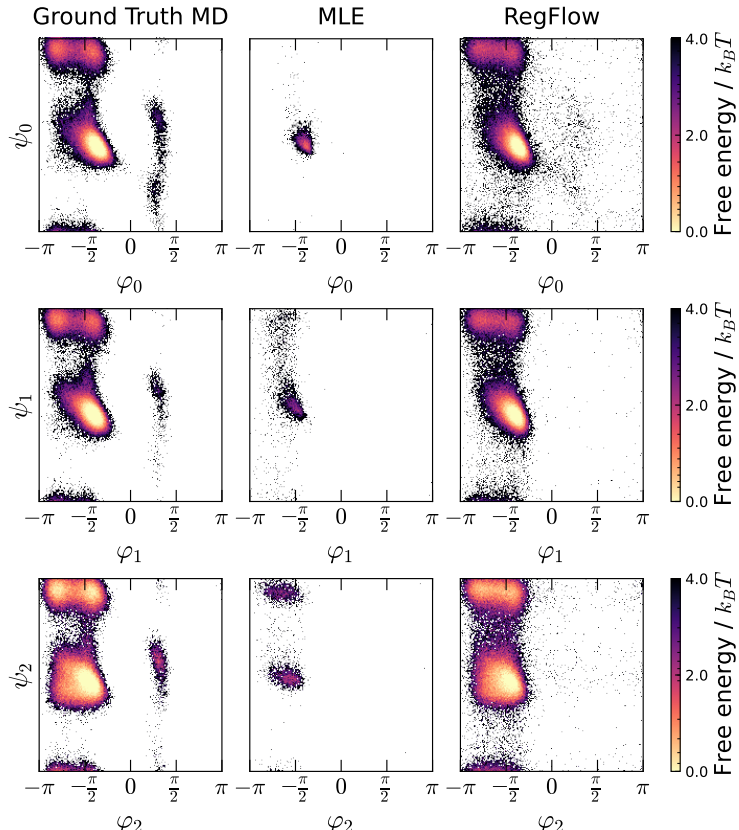
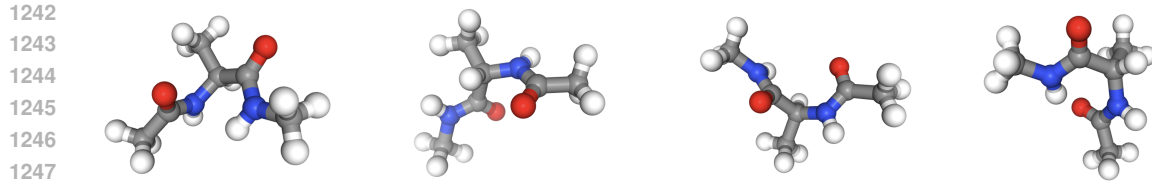


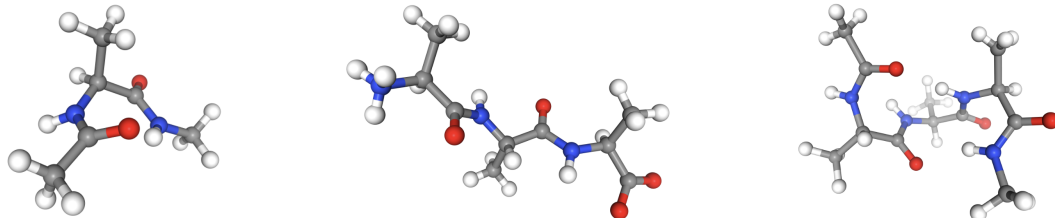
Figure 12: Ramachandran plots for alanine tetrapeptide (**left**: ground truth, **middle**: best MLE-trained flow, **right**: best REGFLOW flow). REGFLOW captures most modes, while MLE-trained flows struggle.

#### D.4 TARGETED FREE ENERGY PERTURBATION

**Generating regression targets.** Using the available MD data, two conformations of alanine dipeptide were selected:  $\beta_{\text{planar}}$  and  $\alpha_R$  (Ghamari et al., 2022). The  $(\phi, \psi)$  ranges for the  $\beta_{\text{planar}}$  conforma-



1248 Figure 13: Generated conformations of alanine dipeptide across various flow-based methods (**left**: NSF w/ MLE;  
1249 **center left**: NSF w/ REGFLOW; **center right**: Res-NVP w/ REGFLOW; **right**: Jet w/ REGFLOW.



1257 Figure 14: Generated samples of larger peptides using NSF (REGFLOW) (**left**: ALDP; **center**: AL3; **right**: AL4).

1258  
1259  
1260  
1261  
1262  
1263  
1264  
1265  
1266  
1267  
1268  
1269  
1270  
1271  
1272  
1273  
1274  
1275  
1276  
1277  
1278  
1279  
1280  
1281  
1282  
1283  
1284  
1285  
1286  
1287  
1288  
1289  
1290  
1291  
1292  
1293  
1294  
1295

tion were chosen as  $(-2.5, -2.2)$  and  $(2.3, 2.6)$ , and for the  $\alpha_R$  conformation as  $(-1.45, -1.2)$  and  $(-0.7, -0.4)$ , respectively. The dataset was then truncated to 82,024 source-target conformation pairs, which were used to compute the OT pairing and generate an invertible map. These pairs were subsequently trained using REGFLOW, with the same model configurations and settings outlined in table 9.